

**KERNFORSCHUNGSZENTRUM  
KARLSRUHE**

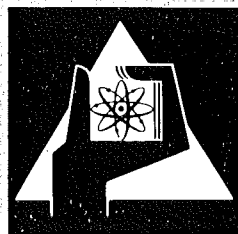
September 1974

KFK 2065

Institut für Angewandte Kernphysik

**Elastic and Inelastic Scattering of Alpha Particles  
and the Folding Model**

H. Rebel



**GESELLSCHAFT  
FÜR  
KERNFORSCHUNG M.B.H.**

**KARLSRUHE**

Als Manuskript vervielfältigt

Für diesen Bericht behalten wir uns alle Rechte vor

GESELLSCHAFT FÜR KERNFORSCHUNG M. B. H.  
KARLSRUHE

KERNFORSCHUNGSZENTRUM KARLSRUHE

KFK 2065

Institut für Angewandte Kernphysik

ELASTIC AND INELASTIC SCATTERING OF ALPHA PARTICLES  
and  
THE FOLDING MODEL

Heinigerd Rebel

Gesellschaft für Kernforschung m.b.H., Karlsruhe

Lectures presented at the International School of  
Nuclear Physics, Predeal, Romania, 4.-13.9.1974



## Abstract

A microscopic approach generating the optical potential by folding an adequate bound-nucleon-projectile effective interaction into the nucleon density distribution has been reviewed for elastic and inelastic scattering of  $\alpha$ -particles.

## Zusammenfassung

Es wird ein Überblick über ein mikroskopisches Streumodell gegeben, welches das optische Potential für die elastische und inelastische Streuung von  $\alpha$ -Teilchen durch eine Faltung einer geeigneten effektiven Wechselwirkung zwischen Projektil und gebundenen Nukleonen mit der Nukleonenverteilung des Targets erzeugt.

## I. Introduction

The determination of nuclear shapes and sizes is one of the traditional problems of nuclear physics. The extent to which we are able to make precise and detailed statements about the nuclear matter distribution reflects the state of our understanding of the nature of the interactions between nuclear particles and of their role in scattering phenomena and stable systems. From electromagnetic measurements, we have a great deal of information about the distribution of protons in nuclei while measurements of the neutron distribution are hampered by a lack of understanding of the strong interactions. In these lectures we are concerned primarily with the extraction and interpretation of nuclear size and shape information from the study of scattering of  $\alpha$ -particles from nuclei. The study of the scattering of  $\alpha$ -particles by atomic nuclei has received extensive and continuous attention in nuclear physics from the very beginnings of the subject. The dominant feature which provides the key for understanding of the most striking phenomena is the strong absorption of the  $\alpha$ -particles at the nuclear surface. The differential scattering cross sections observed at forward angles and at energies above the Coulomb barrier exhibit distinct diffraction like patterns which are qualitatively well represented in terms of models corresponding to a strongly absorbing sphere [Bl 54]. Due to the strong absorption in the nuclear interior most of those  $\alpha$ -particles that are elastically or inelastically scattered are involved in a surface interaction. Thus,  $\alpha$ -particle scattering is generally insensitive to the interaction in the interior region and the role of the nuclear surface is emphasized. This statement is valid, at least for the scattering into the forward hemisphere ("diffraction region"). Indeed, in spite of our ignorance of details of the projectile-nucleus interaction reactions with strongly absorbed projectiles provide some of the most reliable information about nuclear surface properties.

In the past few years  $\alpha$ -particle scattering has been measured at higher bombarding energies up to 166 MeV, and in some cases over more extensive angular ranges thus probing deeper into the nucleus. Thereby some new features have been observed which are not due to the strong absorption and, for example, eliminate ambiguities of the  $\alpha$ -particle scattering interaction potential. These features will not be discussed here. Some remarks concerning the elimination of discrete ambiguities in the nuclear optical potential are given in the appendix. Furthermore, we do not enter in any discussion of phenomena as "anomalous large angle scattering" or intermediate structure effects observed at lower energies and refer for this to [Bud 74]. Our aspects will be confined to  $\alpha$ -particle scattering probing the nuclear surface. In particular, I will report and discuss recent  $\alpha$ -particle scattering studies which used a microscopic or semimicroscopic model - the folding model - as basis of the analyses of the measured cross sections in order to relate the measured quantities to the properties of the nuclear density distribution in a more direct way than the usual phenomenological optical model, namely by generating the real part of the optical potential by folding an adequate effective bound - nucleon - projectile interaction into the nucleon density distribution.

We start with a reminder of the general procedure describing scattering cross sections and a brief description of the traditional basis for the analysis of elastic and inelastic scattering.

## II. Extended optical model description

For many years now it has been customary to describe the scattering from nuclei of nuclear particles in terms of an average (complex) potential well - the optical potential - whose shape because of the short range of the nuclear forces is of the same general form as that of the nuclear density distribution. Various low-lying excited states of nuclei are pictured as corresponding to vibrations of shape or rotations of a deformed shape. It is natural to suppose the optical potential would follow the shape of the density distribution and also become nonspherical. This is taken into account by an adequate parametrisation of the angular dependence of the radius parameter  $R$  (half-way radius) characterizing the spatial extension of the optical potential  $U(\vec{r}_\alpha - R(\Omega))$ , e.g. by the usual expansion

$$R = R_0 \left( 1 + \sum_{\ell m} \alpha_{\ell m} Y_{\ell m}(\Omega) \right)$$

This expansion defines the collective coordinates and provides a coupling whereby incident particles can be inelastically scattered and excite the corresponding collective modes of the target nucleus. Such an approach has been very successful in fitting the experimental data: the measured cross sections and strongly oscillating angular distributions. The analysis of the experiments extracts the coupling strengths: matrix-elements of the transition operators which are built up by the collective coordinates and are usually called deformation parameters.

In general we are interested not only in the absolute values of these deformation parameters but also in their signs (relative phase). In the case of a permanent deformation we may parametrize  $R$  in the body fixed system

$$R = R_0 (1 + \beta_2 Y_{20}(\Omega') + \beta_4 Y_{40}(\Omega'))$$

assuming axial symmetry and including a hexadecapole deformation. The sign of the intrinsic quadrupole deformation parameter  $\beta_2$  characterizes the nuclear shape as being prolate or

oblate. In the case of a triaxial shape

$$R = R_0(1 + \beta \cos \gamma Y_{20}(\Omega') + \frac{1}{\sqrt{2}} \beta \sin \gamma [Y_{22}(\Omega') + Y_{2-2}(\Omega')])$$

with the usual parameters  $\beta$  and  $\gamma$  introduced by Bohr, the asymmetry angle  $\gamma$  is a convenient measure of a triaxial quadrupole deformation of the nucleus.

From our experiments with 104 MeV  $\alpha$ -particles [Re 72a, Re 72b] we have learned that the differential cross sections measured with sufficient accuracy will inform also on such details: signs of intrinsic deformation, deviation of axial symmetry and  $Y_4$ -components of the deformation. This information is due to the pronounced interference of single and higher order excitation processes which influence by typical features the observed distinct diffraction pattern in magnitude, slope and phase of the diffraction oscillations. In principle, multiple step processes may also distinguish between a permanent deformation and collective vibration though this may be somewhat academic in regard on the softness of most nuclei.

It is worthwhile to remind of some implications of multiple excitation processes for nuclear structure studies. Their presence or absence places severe restrictions on the nuclear model in question. Consider a  $4^+$  excited state as a member of the ground state rotational band. The amount of  $L=4$  single excitation admixture (to the expected double excitation contribution) is a measure of magnitude and sign of the intrinsic  $Y_4$ -deformation. The enhancement for the excitation of the  $4^+$  states affects also the excitation of the  $2^+$  state by higher order processes. In this way the differential cross sections become the results of a delicate interference between single and higher order excitation. In fig. 2 various coherent amplitudes are represented by corresponding "graphs".

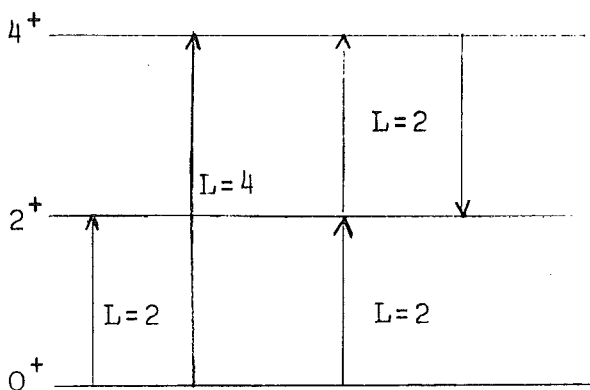


Fig. 1: Some possible first and second order excitation processes. The cascade processes compete with direct transitions causing interferences which can be observed in the measured cross sections. The leading terms for the  $L=2,4$  matrix elements are proportional to  $\beta_2$  and  $\beta_4$ , respectively.

For the analysis of the interference processes the pronounced oscillation structure of the  $\alpha$ -particle scattering cross sections is very useful. It is obvious that high bombarding energies are advantageous. If the energy is sufficiently high the "grazing"  $\alpha$ -particles carry a high enough momentum so that large direct momentum transfer is possible. This is a necessary feature for a study of higher multipole moments (L) since such a study becomes only possible when direct excitation of the I=L member of the band contributes significantly. On the other hand, with increasing energy the contribution of higher order processes is enhanced as we may learn from simpler reaction models, e.g. the Austern-Blair model [Au 65]. In order to extract the information hidden in the measured cross sections we need an analysing method which considers all coherent excitation paths and takes into account of all important couplings via intermediate states. This is provided by the coupled channel method.

The basic procedure is the following:

The wave function  $\psi_i^{(+)}(\vec{r}_\alpha, \xi)$  which solves the scattering problem on the basis of the assumed scattering model (represented by the interaction potential  $U(\vec{r}_\alpha, \xi)$ ) is expanded into a complete set of projectile-target-eigenfunctions  $\phi_n(\xi)$

$$\psi_i^{(+)}(\vec{r}_\alpha, \xi) = \sum_{n'} \psi_{n'}^{(+)}(\vec{r}_\alpha) \phi_{n'}(\xi)$$

The Schrödinger equation is equivalent to an infinite set of coupled equations for the channel amplitudes  $\psi_{n'}^{(+)}(\vec{r}_\alpha)$ . For the channel n we have

$$(E - \epsilon_n - K - U_{nn}) \psi_n^{(+)}(\vec{r}_\alpha) = \sum_{n' \neq n} U_{nn'} \psi_{n'}^{(+)}(\vec{r}_\alpha)$$

The quantities  $U_{nn'} = \langle \phi_n | U | \phi_{n'} \rangle$  are the matrix elements of the interaction.

The coupling of different channels via the nondiagonal matrix elements  $U_{nn'}$  is obvious.

The sum over  $n'$  runs over all continuum states as well as the bound states. In praxi we assume that, for a given channel n, only a few channels  $n'$  are strongly coupled and that the remainder need not be included explicitly. They are not ignored entirely, however. Their elimination is compensated by replacing U by an optical potential. This effective interaction is now a matrix in the subspace of the chosen nuclear instead of being diagonal as with the more familiar optical potential.

The DWBA is restricted to couplings to the ground state and neglects the excitation via intermediate states. As well known this is not adequate for inelastic scattering as well as for some types of reactions [Asc 71].

For coupled channel calculations several effective computer codes [e.g. Ta 67, Schwei 13] are available.

The physics of the system is represented by the coupling matrix elements. For  $\alpha$ -particle scattering at higher energies nuclear excitation is dominant and Coulomb excitation is less important. It should be emphasized that our ignorance of the nuclear interaction and the various approximations which lead to an effective interaction may introduce a model dependence by the specific choice of the parametrization of the effective interaction. This type of model dependence is in addition to the dependence of the structure model of the nuclear states  $|n\rangle$  and  $|n'\rangle$ . There we find a principal difference from the starting point of the analysis of electromagnetic processes. For Coulomb excitation e.g. the matrix elements  $U_{nn'}$ , say  $B(E2)$ -values or static moments, are nearly "model independent" and suitable for further interpretation. In the case of nuclear excitation, however, it is usual to generate the matrix elements from a model of the states and a model of the interaction. On this basis there is a very successful tradition to derive the form factors from a phenomenological complex potential deformed in an adequate way.

Two examples may demonstrate the sensitivity of the  $\alpha$ -particle scattering to the shape of this "extended optical potential".

- a) Fig. 2 presents a results of systematic studies of hexadecapole deformations of 2s-1d shell nuclei [Re 72b]. The theoretical curves are full coupled channel calculations using a rotational model for  $^{20}\text{Ne}$ . The different theoretical curves demonstrate the sensitivity to magnitude and sign of  $\beta_4$ . The best fit value of  $\beta_4$  corresponds to a branching ratio of E4 to E2-cascade decay of about  $10^{-8}$ .
- b) The second example illustrates prolate-oblate effects of the scattering cross sections. These effects result from the interference processes and are qualitatively predicted by the simple diffraction model including second order terms in the deformation parameters [Re 72a].

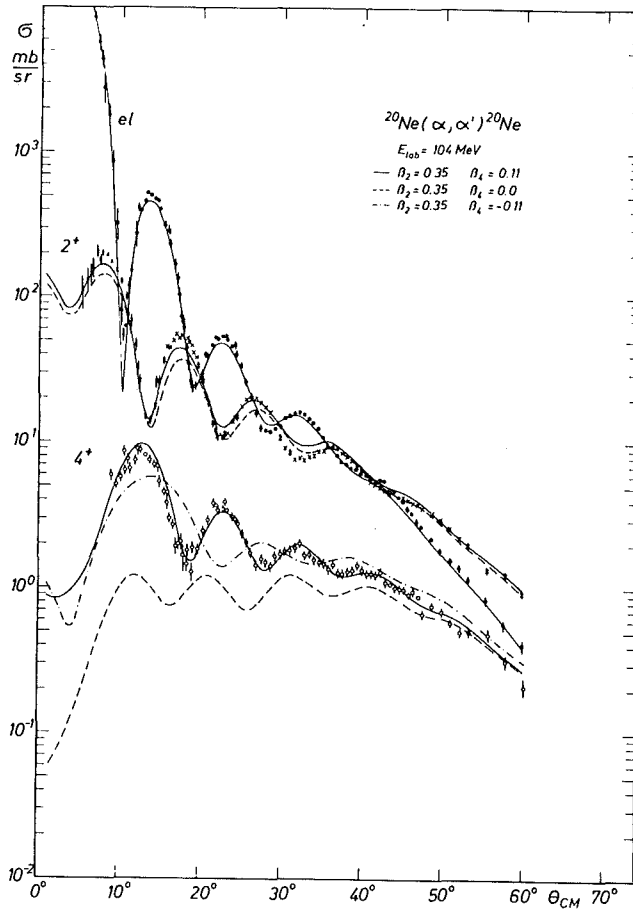


Fig. 2: Demonstration of the sensitivity of elastic and inelastic scattering of 104 MeV  $\alpha$ -particles to hexadecapole deformations. The theoretical curves are full coupled channel calculations on the basis of the rotational model (including Coulomb excitation).

In a first order diffraction model the structure of the angular distributions is approximately given by a term proportional to  $\cos^2(x + \pi/4)$  for the elastic scattering, by a term proportional to  $\sin^2(x + \pi/4)$  for the  $2_1^+$ -angular distribution ( $x \approx \pi$ ). Here  $x = k R \theta$ ,  $k$  = wave number and  $\theta$  the scattering angle. Including second order excitation the  $2_1^+$ -cross section is modified, not only the amplitude but also the oscillation behaviour by a modulation factor  $\Delta\omega$ .

The approximate expression for the region near the elastic maxima we have

$$\frac{d\sigma}{d\Omega}(0^+ \rightarrow 2_1^+) \propto \sin^2((1 + \gamma)x + \pi/4)$$

Here the quantity  $\gamma$  is dependent on the quadrupole deformation parameter linearly ( $\gamma \approx \beta_2/10$ ). The sign of  $\beta_2$  leads to the following effects:

- (i) A shift  $\epsilon$  of the position of the  $2_1^+$  cross section relative to the elastic minima

$$\epsilon \propto -\frac{1}{4} \pi \gamma$$

- (ii) A modification of the oscillation period of the inelastic scattering cross section:

$$\omega_{inel} = 1 + \gamma \left. \begin{array}{l} > \omega_{el} \text{ in the prolate case} \\ < \omega_{el} \text{ in the oblate case} \end{array} \right\}$$

These prolate-oblate effects, which become apparent for sufficiently large k-values are reproduced by exact coupled channel calculations.

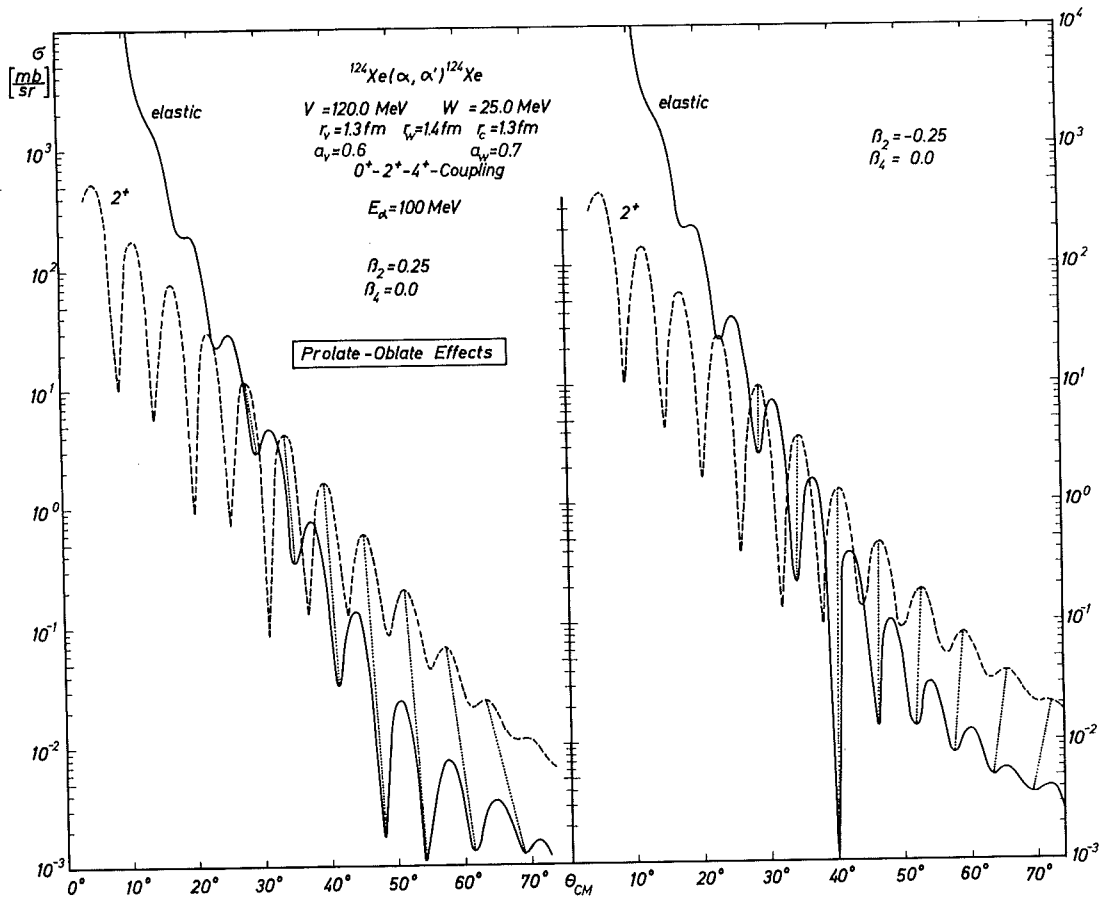


Fig. 3: Demonstration of prolate-oblate effects: Coupled channel calculations of  $^{124}\text{Xe}(\alpha, \alpha')^{124}\text{Xe}$  at  $E_\alpha=100$  MeV for positive and negative intrinsic permanent quadrupole deformation  $\beta_2$  of the extended optical potential [Re 72a]

Fig. 3 shows typical results of coupled channel calculations of the differential cross sections for elastic and inelastic scattering of 100 MeV  $\alpha$ -particles from  $^{124}\text{Xe}$ . These calculations are based on the assumption that the interaction of the  $\alpha$ -particles can be represented by a deformed complex optical potential. The effects are evident and can provide a reliable determination of the sign of the quadrupole deformation.\*)

For example we quote results for 104 MeV  $\alpha$ -particle scattering from  $^{20}\text{Ne}$  and  $^{28}\text{Si}$ . The coupled channel analyses resulted in a prolate shape of  $^{20}\text{Ne}$  and an oblate shape of  $^{28}\text{Si}$  [Re 72b]. This agrees with results of the reorientation in Coulomb excitation [cf. Schwa 72].

There are similar and some what more striking effects in the oscillation pattern of the  $2_2^+$  cross section which informs on the  $\gamma$ -deformation in the case of a asymmetrically deformed optical potential [Re 73b].

### III. Folding model

From several reasons the traditional description of elastic and inelastic scattering in the framework of the usual optical model is not very satisfactory. The interpretation is highly phenomenological and does not provide any insight into the more microscopic aspects of the reaction and excitation mechanism. From microscopic point of view we seek to describe the scattering of the projectile from a nucleus in terms of more fundamental interactions between the nucleons in order to gain an understanding of the interactions starting from the nucleon-nucleon force and in terms of motions of individual nucleons. In all aspects this is a very ambitious project because of the features of the nuclear forces (indistinguishability and repulsive part) and of the many body problem. But even if we transform the

---

\*) Extensive studies of these effects already predicted by diffraction theory of Inopin [In 67] have been performed by V. Yu. Gonchar et al. [Gon 71]. This came to the author's knowledge just recently.

original problem in a problem of a system of particles interacting via an "effective interaction" and are satisfied with a phenomenological description of size and shape of the nucleus and, in particular, of its collective modes, the macroscopic optical model basis is insufficient as it represents already a convolution of the properties of the target nucleus and the test-particle. There is no reason that different types of projectiles illuminate the target nucleus by the same coloured light. Therefore it is not surprising that, in fact, values of the deformation parameters extracted from scattering of electrons, nucleons,  $\tau$ - and  $\alpha$ -particles are systematically different and apparently indicate discrepant transition rates. The size and deformation parameters provided by the traditional analysis characterize the interaction potential. The connection between these parameters (as well as between the strong absorption radius which seems to be a significant size parameter) and the nuclear matter distribution is unclear.

A scaling relation

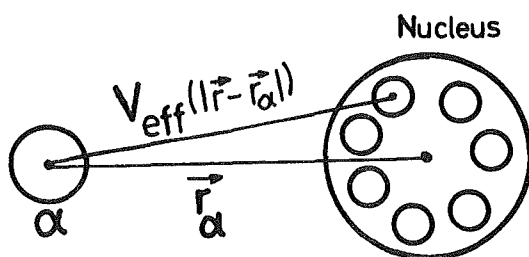
$$R_L^{\text{mass}} \cdot R^{\text{mass}} = R_L^{\text{Pot}} \cdot R^{\text{Pot}}$$

has been proposed by Blair [Bl 60, Au 65] and is widely used [cf. Bern 69] in order to relate the potential deformation to the deformation of the mass distribution. The radius  $R^{\text{mass}}$  may be taken from electron scattering results. Such a recipe seems to be too simple and does not remove all discrepancies.

Thus, if we are interested in properties of the nuclear density distributions it is obviously more reasonable to formulate the scattering model in terms of the matter or nucleon distributions. Such a procedure is provided by the folding model. We endeavour here to review  $\alpha$ -particle scattering studies on the basis of this model and to indicate the areas of confidence and uncertainty in determination size and shapes of nuclei.

To lowest order of a multiple scattering expansion [Jack 69] the real part  $U_R(\vec{r}_\alpha)$  of the optical potential is generated by averaging an effective projectile-bound-nucleon interaction  $V_{\text{eff}}(\vec{r}_\alpha, \vec{r})$  over the nucleon density distribution of the target.

$$\rho(\vec{r}) = \rho_p(\vec{r}) + \rho_n(\vec{r}) = \langle 0 | \sum_{i=1}^A \delta(\vec{r} - \vec{r}_i) | 0 \rangle$$



Thus, we have a most simple and intuitive expression defining the model:

$$U_R(\vec{r}_\alpha) = \int V_{\text{eff}}(\vec{r}_\alpha, \vec{r}) \rho(\vec{r}) d^3r$$

The finite size of the projectile is taken into account through the range of the potential  $V_{\text{eff}}$ , but the polarizability of the projectile is neglected. The  $L=0$  term generated by the multipole expansions of  $V_{\text{eff}}(\vec{r}_\alpha, \vec{r})$  and  $\rho(\vec{r})$  defines the spherical part of the optical potential for elastic scattering.

Since this model for the optical potential does not explicitly include the effects of virtual transitions the calculated potential should strictly be compared with the spherical potential used in coupled channel calculations rather than the optical potential which fit the elastic data when coupling is neglected.

A number of interesting relationships arise from the folding expression [Jack 74]. The mean square radii of the potential ( $U$ ), the effective interaction ( $V$ ) and the density distribution obey the relation

$$\langle r^2 \rangle_U = \langle r^2 \rangle_V + \langle r^2 \rangle_\rho$$

Starting from the folding expression Greenlees and coworkers [Green 68] have reformulated the optical model of elastic proton scattering. They showed that the real part of the optical model potential is a possible source of information regarding the sizes of nuclei.

It is not unreasonable to apply such a "microscopic" treatment of the optical potential to the scattering of tightly bound composite projectiles. A quantitative use of this method will depend on the precision with which we can define the interaction

$V_{\text{eff}}(\vec{r}_\alpha, \vec{r})$  between the free  $\alpha$ -particle and a target nucleon. As result of the general scattering theory we know that the effective potential would be energy-dependent, nonlocal and complex and differs from the free interaction by an infinite sum of terms over all allowed intermediate states of the system [Sat 67, Glen 67]. In a local approximation  $V_{\text{eff}}$  should be treated as a phenomenological interaction which simulates some of the many-body effects. Their parameters may therefore be determined by fitting the data of  $\alpha$ -particle scattering by nuclei [Morg 69, Tat 70, Bern 71, Lern 72]. It may be argued the interaction of the  $\alpha$ -particle with the nucleus is confined to a region where the nucleon density is low so that, unless substantial clustering occurs, the effect of exchange and multiple scattering may be very much reduced compared with the situation for nucleon-nucleus scattering. This would imply that  $V_{\text{eff}}(\vec{r}_\alpha, \vec{r})$  should be very similar to the free nucleon  $\alpha$  interaction [Mad 65, Lil 71, Mail 72, Mail 73]. Such phenomenological potentials which fit nucleon- $\alpha$  scattering implicitly include the effects of exchange between a target nucleon and one within the  $\alpha$ -particle. They are successfully applied in folding model analyses of elastic scattering, especially at lower energies (near the Coulomb barrier) and reproduce even the features of the scattering at large angles [Mail 72, Mail 73, Sin 74].

An objection to the use of simple phenomenological potentials for  $\alpha$ -nucleon scattering arises from the fact that these potentials allow a bound 1s-state for the 5-body system which is forbidden by the exclusion principle. This objection would not apply to calculations in the resonating group formalism in which the  $\alpha$ -nucleon interaction is derived from the nucleon-nucleon interaction.

Another approach is to use a double folding procedure and derive the  $\alpha$ -nucleon interaction by averaging the nucleon-nucleon interaction over the internal motion of the  $\alpha$ -particle [Glen 66, Bern 69, Bud 70, Batt 71a] requiring some adjustment to take into account of exchange effects. These approaches have been compared by Batty et al. [Batt 71b] with the conclusion that the best choice for a local effective interaction is the simple Gaussian form

$$V_{\text{eff}} = V_0 \exp \left[ -|\vec{r} - \vec{r}_\alpha|^2 / \mu_0^2 \right]$$

The calculated parameters give reasonable agreement with the nucleon- $\alpha$ -scattering and are also successfully used in low- and medium energy  $\alpha$ -scattering analyses. A Saxon-Woods form improves the agreement with nucleon- $\alpha$ -scattering [Sat 68, Mail 72] but is less satisfactory for inelastic scattering [Sat 71a].

For most of the following demonstrations we use the Gaussian interaction in the form

$$V_{\text{eff}} = \lambda_R V_0 \exp \left[ -|\vec{r} - \vec{r}_\alpha|^2 / \mu_0^2 \right]$$

with  $V_0 = -37$  MeV and  $\mu_0 = 2$  fm [Bern 69]. The energy dependent factor  $\lambda_R$  takes into account of the "renormalisation" due to the presence of the other bound nucleons. Its value has the order of magnitude of 1 and is determined phenomenologically thus absorbing some uncertainties. The effective interaction should be in principle complex [Fes 58]. We know that for medium energies and restricted angular range the  $\alpha$ -scattering data are not very sensitive to the detailed form of the imaginary part of the optical potential. A macroscopic four-parameter optical potential is often sufficient. Therefore an imaginary part  $U_I(\vec{r}_\alpha)$  of the same form as the real potential can be used with excellent results [Morg 69, Batt 71a, Bern 71, Bern 72, Tat 70, Re 72c]. Introducing a further parameter  $\lambda_I$  we write

$$U(\vec{r}_\alpha) = (\lambda_R + i \lambda_I) \int V_0 \exp(-|\vec{r} - \vec{r}_\alpha|^2 / \mu_0^2) \cdot \rho(r) d^3r$$

Alternatively an independent parametrisation (the macroscopic Saxon-Woods-form) of the imaginary part has been used [Mail 72, Mail 73, Re 72c, Gi 74].

There are always two components in calculations of the type discussed here. One is the effective  $\alpha$ -nucleon interaction  $V_{\text{eff}}$ , the other is the target nucleus density distribution  $\rho$ . In order to learn something about the former, we need to reduce to a minimum the uncertainties concerning the latter. Batty et al. [Batt 71b] fitted the 42 MeV data of Fernandez and Blair [Fe 70] for the calcium and nickel isotopes and used nuclear matter distributions derived from single particle wave functions generated by reliable bound state potentials [cf. Batt 71b]. Examination

of the corresponding optical potentials shows that the search procedure adjusts the free parameters to give the same real potential in the vicinity of the strong absorption radius. This leads to an ambiguity in the form

$$\lambda_R \cdot V_0 \cdot \mu_0^6 = \text{const}$$

The constant depends on the type of nuclear density distribution used. This shows also the dependence of the phenomenologically derived effective interaction on the uncertainties of the specific nuclear density distribution which we use as "calibration-standard".

Another approach [Bern 71, Bern 72] has taken the view that nuclei with  $N=Z$  should be used to determine the parameters of an effective interaction. For  $T=0$  nuclei it can be assumed that the neutron distribution  $\rho_n$  and the proton distribution  $\rho_p$  are approximately equal and can be obtained from electron scattering experiments. Using a gaussian interaction with  $\mu_0 = 2.0$  fm Bernstein and Seidler [Bern 71] fitted the 104 MeV elastic  $\alpha$ -particle scattering from  $^{40}\text{Ca}$  [Haus 69] and then predicted the cross sections for  $^{16}\text{O}$  and  $^{28}\text{Si}$  without further variation of the parameters. Results of these calculations and the experimental cross sections measured by the Karlsruhe group [Haus 69, Re 72b] are displayed in Fig. 3.

Bernstein et al. [Bern 72] subsequently examined scattering from  $^{90}\text{Zr}$  and  $^{208}\text{Pb}$  at  $E_\alpha = 104$  MeV and determined parameters of a nuclear matter distribution of fermi shape

$$\rho(r) = \rho_0 / (1 + \exp [(r-c_m)/a_m])$$

Combining the results with parameters for the proton distribution taken from electron scattering they obtain  $\langle r^2 \rangle^{1/2}_n - \langle r^2 \rangle^{1/2}_p = 0.20 \pm 0.13$  fm for  $^{90}\text{Zr}$  and  $0.26 \pm 0.13$  fm for  $^{208}\text{Pb}$ . Is this an indication for a thin neutron skin for heavier nuclei?

Elastic Scattering of 104 MeV  $\alpha$ -Particles  
Folding Model

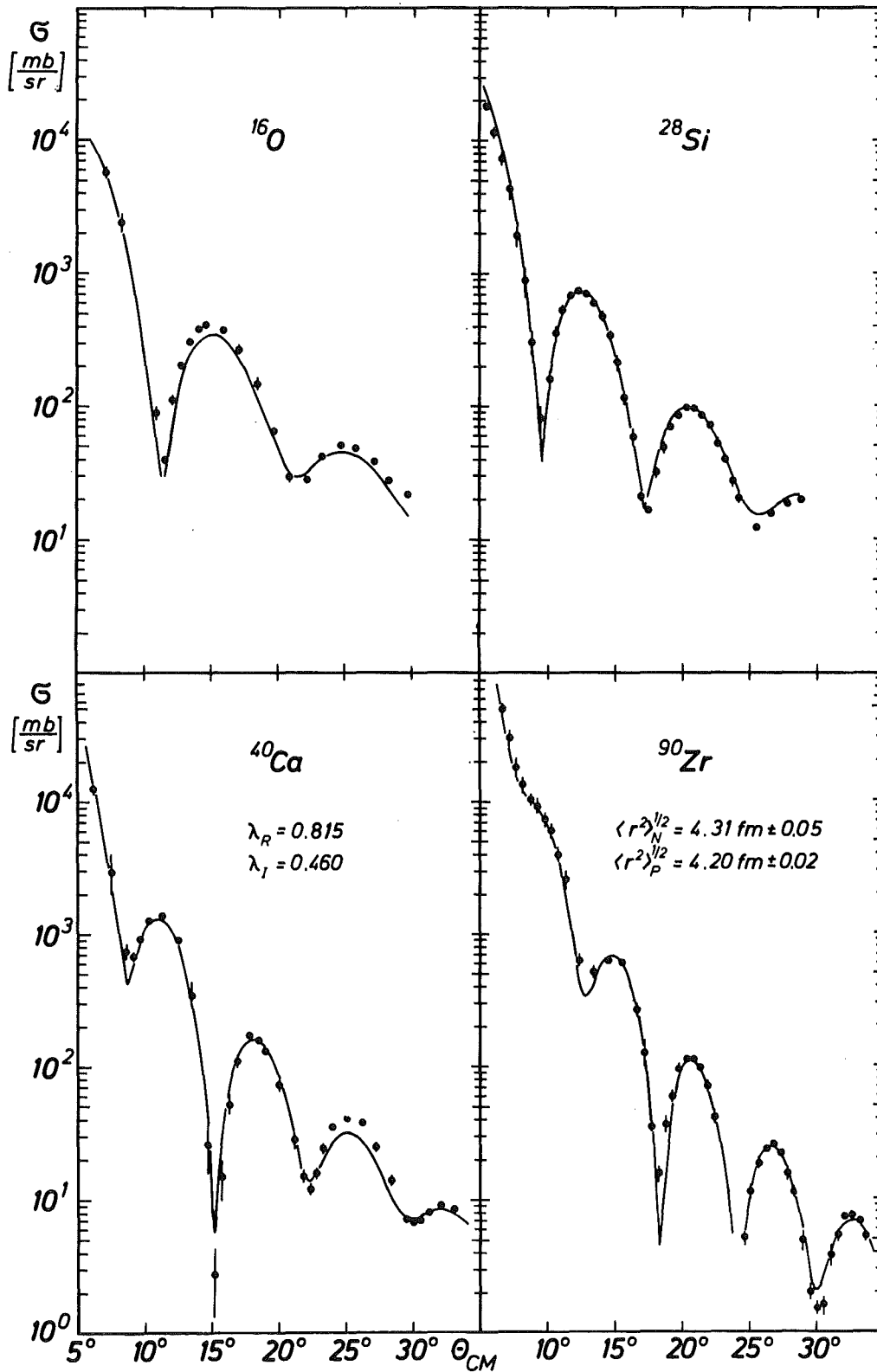


Fig. 4: Folding model of elastic scattering of 104 MeV  $\alpha$ -particles using a Gaussian effective interaction which has been determined by fitting  $^{40}\text{Ca}(\alpha, \alpha)^{40}\text{Ca}$  [Bern 71]. Theoretical predictions and experimental results [Haus 69] for the scattering on  $^{16}\text{O}$  and  $^{28}\text{Si}$  - Analysis of  $^{90}\text{Zr}(\alpha, \alpha)^{90}\text{Zr}$  with different density distributions for protons and neutrons [Bern 71].

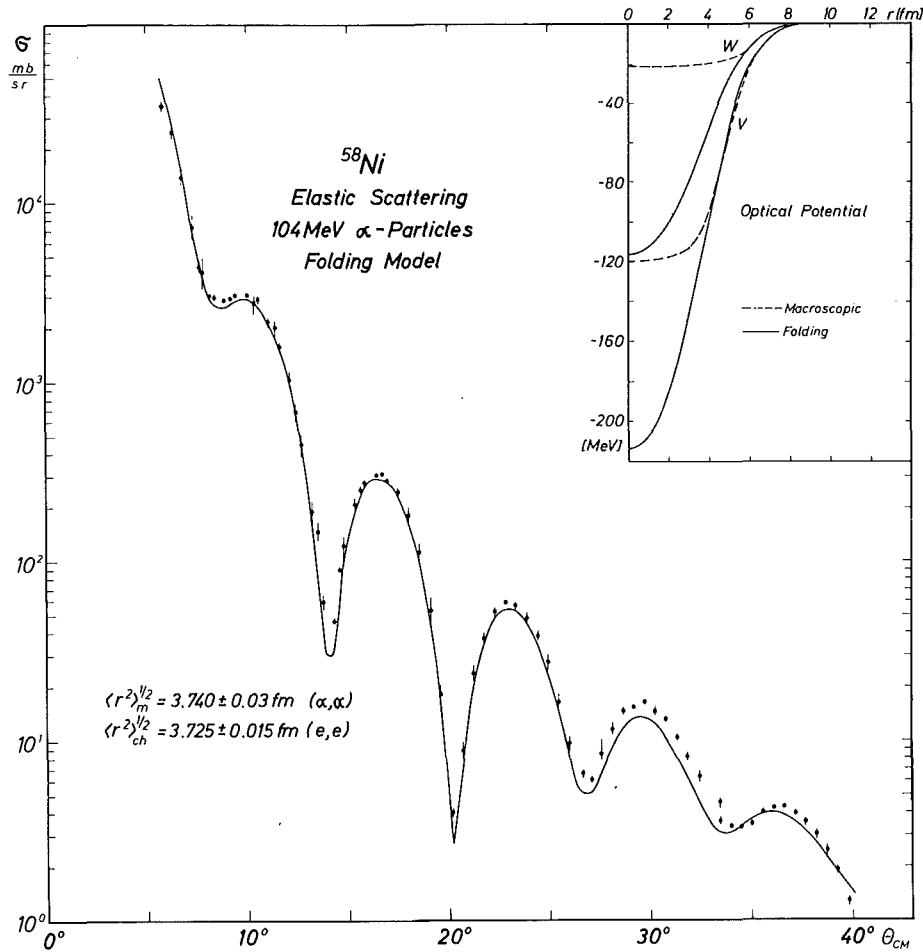


Fig. 5: Folding model analysis of elastic scattering of 104 MeV  $\alpha$ -particles from  $^{58}\text{Ni}$  with corresponding optical potential compared to the phenomenological optical potential [Re 72c]

Fig. 5 presents an example of studies of elastic scattering from the nickel isotopes  $^{58,60,62,64}\text{Ni}$  at  $E_\alpha = 104$  MeV [Re 72c]. The parameters of a fermi distribution have been varied and result in a value of the rms-radius which is in excellent agreement with the experimental results of electron scattering [Fic 70].

Fig. 5 shows also the corresponding optical potential compared to the phenomenological optical potential obtained by the standard analysis. This result is representative for similar studies [Lil 71, Jack 69b] which confirm that the folding procedure can reproduce the required agreement and behaviour for the surface region.

It is known that for low- and medium-energy  $\alpha$ -particles only the potential around the Coulomb barrier or strong absorption radius is well determined [Jack 68, Fe 70]. In this region the nuclear matter density is very low. However, it is not correct to assume that  $\alpha$ -particles probe the matter distribution only in this low density region because of the finite range of  $V_{\text{eff}}$ . An examination of the behaviour of the integrand in the folding formula shows (see fig. 6) that the sensitive region of the potentials is determined mainly by the 10-50 % region of the matter distribution [Batt 71b]. For 104 MeV studies of the spatial region to which the elastic cross sections are sensitive show that this region extends approximately 90 % to 1 % of the central density [Bern 71].

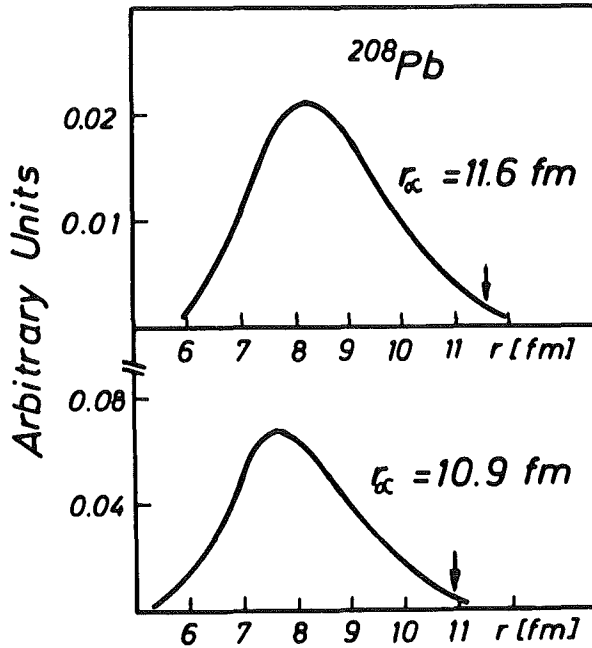


Fig. 6: Integrands of the folding integral

$$U_R(\vec{r}_\alpha) = \int \rho(r) \exp(-|\vec{r}_\alpha - \vec{r}|^2 / \mu_0^2) d\vec{r}$$

near the strong-absorption radius and the Coulomb barrier radius for  $^{208}\text{Pb}$  (from Batt 71b)

A recent criticism [My 73] of the folding method as usually applied suggests that a density-dependent two-body interaction is essential. Such refinements are not expected to affect the studies with particles which only 'taste' the low density region. In some exploratory calculations an effective interaction with a density dependent factor  $(1-g \rho(r)/\rho(0))$  is used. The effect of varying the parameter  $g$  is to reduce the contribution from the inner region. But the experimental data require an adjustment of  $\lambda_R$  or  $V_0$  that the resulting potential remains the same in the surface region [Morg 69, Re 74c].

Recently further semimicroscopic investigations of 104 MeV  $\alpha$ -particle scattering have been performed for  $^{46,48,50}\text{Ti}$  [Re 74a] and  $^{56}\text{Fe}$  [Gi 74] (see fig. 7).

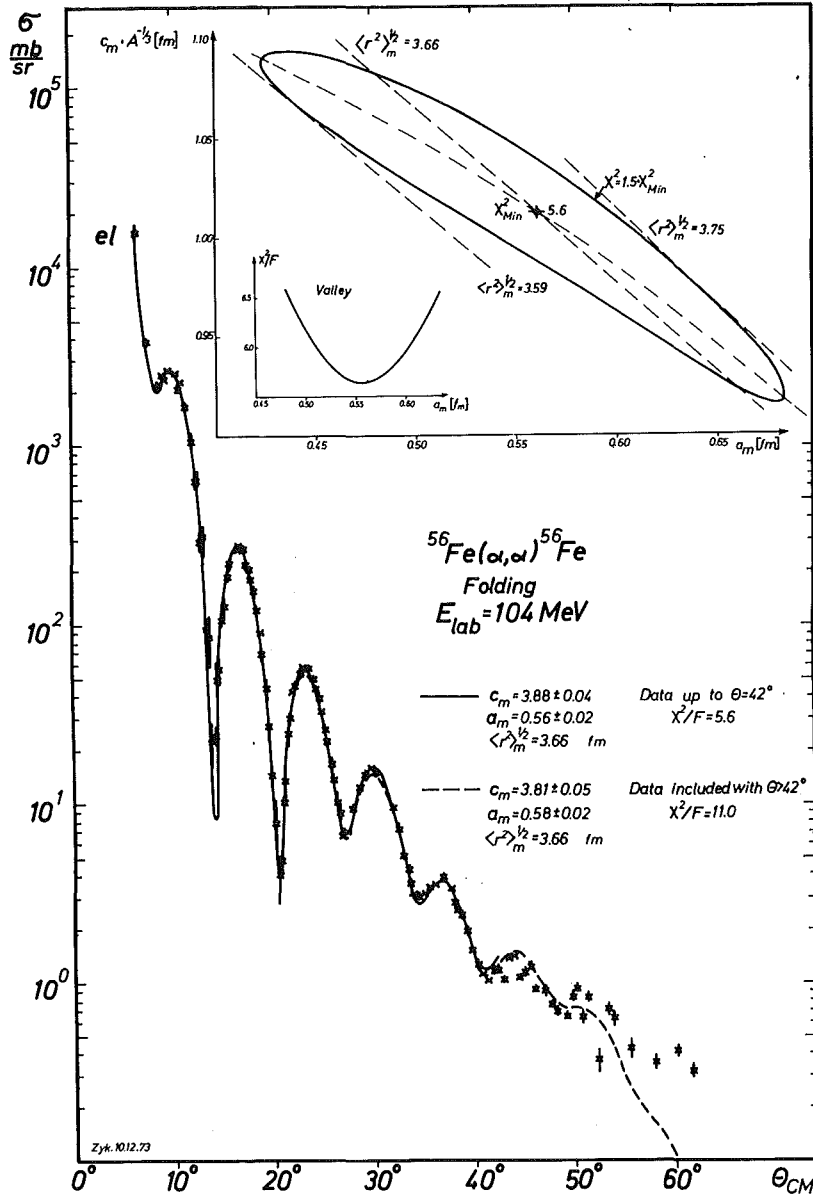


Fig. 7: Folding model analysis of elastic scattering of 104 MeV  $\alpha$ -particles from  $^{56}\text{Fe}$ .  $\chi^2$ -contour plot in the plane of the parameters  $c_m$  and  $a_m$  of the nucleon distribution defining the range of confidence of the extracted values [Gi 74]

Significance and sensitivity of the parameters  $c_m$  and  $a_m$  of the fermi distribution  $\rho$  are studied. Obviously, the rms-radius is much better defined by the experimental data than the correlated value of the half-way radius  $c_m$  and of the diffuseness  $a_m$ . A scan

of  $a_m$  around the best-fit-value requires  $c_m$ -values along the valley of the  $\chi^2$ -landscape. The rms-radius seems to be that moment which is well determined by the elastic scattering.

The same conclusion results from various studies [Bern 72, Weis 70], e.g. of Mailandt et al. [Mail 73] (who used a phenomenological  $\alpha$ -nucleon interaction of Saxon-Woods form).

It should be remarked that the value of the rms-radius  $\langle r^2 \rangle_N^{1/2} = 3.66$  fm is related to the nucleon (- centers -) distribution. \*) The value agrees excellently with the value of the proton distribution which we deduce from the charge radius [Elt 74] by unfolding the charge distribution of the proton via

$$\langle r^2 \rangle_{ch} = \langle r^2 \rangle_p + \langle r^2 \rangle_{Proton}$$

assuming  $\langle r^2 \rangle_{Proton}^{1/2} = 0.8$  fm.

Extensive microscopic calculations have been also carried out at  $E_\alpha = 166$  MeV using a Gaussian interaction with  $\mu_0 = 2.0$  fm. By analysing elastic scattering for a range of nuclei average values of  $\lambda_R$  and  $\lambda_I$  (in our notation) were obtained. The strength factor  $\lambda_R$  decreases, more or less linearly with the incident energy [Tat 70]. This energy dependence has been also systematically investigated by Lerner et al. [Lern 72] for the  $\alpha$ -particle scattering from  $^{40}\text{Ca}$  in the energy range  $E_\alpha = 39.6 - 115.4$  MeV. Further studies at  $E_\alpha = 166$  MeV tried to extract parameters of the neutron distributions using fermi or modified fermi distributions ( $\rho(r) = (1 + w r^2/c_m^2) \cdot \rho_0 (1 + \exp[(r^n - c_m^n)/a_m^n])^{-1}$ ). Tab. 1 (taken from [Bri 72b]) compiles the results for 166 MeV  $\alpha$ -particle scattering and compares with shell model calculations. The results are generally consistent with  $\langle r^2 \rangle_n^{1/2} - \langle r^2 \rangle_p^{1/2} = 0.15 \pm 0.1$  fm.

Some uncertainties of all these results reviewed here arise from the unknown influence of exchange effects. We know from calculations of proton scattering that knock-on terms corresponding

---

\*) In nuclear theory the one-particle density functions for nucleons are usually defined as distributions of point particles in the nucleus.

$R_c$  = rms radius charge distribution  
 $R_p$  = rms radius proton distribution  
 $r_p$  = rms radius of the proton (0.8 fm)

$$R_c^2 = R_p^2 + r_p^2$$

$R_n$  = rms radius neutron distribution

$$R_{n,m}^2 = R_n^2 + r_n^2 \quad (r_n = r_p)$$

$\begin{matrix} A \\ Z \end{matrix} X_N$	Cette expérience				Modèle en couches	
	$R_c$	$R_{n,m}$	$R_p$	$R_n$	$R_p$	$R_n$
$^{12}_6C_6$	2.46	2.46±0.08	2.34	2.34±0.08		
$^{24}_{12}Mg_{12}$	3.02	2.96±0.09	2.91	2.85±0.09	3.07	2.97
$^{28}_{14}Si_{14}$	3.13	3.04±0.09	3.04	2.94±0.09	3.15	3.07
$^{32}_{16}S_{16}$	3.25	3.24±0.10	3.15	3.14±0.10	3.27	3.18
$^{40}_{20}Ca_{20}$	3.49	3.43±0.12	3.41	3.34±0.12	3.43	3.31
$^{44}_{20}Ca_{24}$	3.52	3.61±0.16	3.43	3.52±0.16	3.44	3.51
$^{48}_{20}Ca_{28}$	3.48	3.81±0.12	3.39	3.72±0.12	3.40	3.65
$^{48}_{22}Ti_{26}$	3.58	3.53±0.12	3.49	3.44±0.12	3.50	3.59
$^{56}_{26}Fe_{30}$	3.75	3.70±0.11	3.67	3.62±0.11	3.70	3.76
$^{59}_{27}Co_{32}$	3.75	3.85±0.11	3.66	3.76±0.11	3.74	3.83
$^{58}_{28}Ni_{30}$	3.73	3.74±0.10	3.65	3.66±0.10	3.77	3.76
$^{60}_{28}Ni_{32}$	3.75	3.83±0.10	3.67	3.75±0.10	3.78	3.83
$^{62}_{28}Ni_{34}$	3.79	3.88±0.10	3.71	3.80±0.10	3.79	3.88
$^{68}_{30}Zn_{38}$	3.92	4.04±0.15	3.84	3.96±0.15	3.87	4.00
$^{88}_{38}Sr_{50}$	4.25	4.42±0.16	4.18	4.35±0.16	4.15	4.30
$^{89}_{39}Y_{50}$	4.28	4.41±0.10	4.21	4.34±0.10	4.17	4.30
$^{90}_{40}Zr_{50}$	4.27	4.27±0.12	4.19	4.19±0.12	4.20	4.31
$^{94}_{40}Zr_{54}$	4.34	4.46±0.11	4.27	4.39±0.11	4.22	4.44
$^{92}_{42}Mo_{50}$	4.33	4.33±0.09	4.26	4.26±0.09	4.27	4.32
$^{116}_{50}Sn_{66}$	4.60	4.68±0.09	4.53	4.61±0.09	4.57	4.70
$^{118}_{50}Sn_{68}$	4.62	4.79±0.09	4.55	4.72±0.09	4.58	4.73
$^{120}_{50}Sn_{70}$	4.64	4.87±0.09	4.57	4.80±0.09	4.59	4.76
$^{124}_{50}Sn_{74}$	4.67	4.83±0.09	4.60	4.76±0.09	4.62	4.84
$^{140}_{58}Ce_{82}$	4.88	4.97±0.10	4.82	4.91±0.10	4.83	4.98
$^{208}_{82}Pb_{126}$	5.50	5.75±0.09	5.44	5.69±0.09	5.48	5.68

Les valeurs de  $R_p$  et  $R_n$  calculées par Beiner avec un modèle en couches sont données pour les noyaux étudiés

from I. Brissaud et al.

Tab. 1: A compilation of folding model results for elastic scattering of 166 MeV  $\alpha$ -particles [from Bri 72b]

to exchange of the incident proton with a target nucleon can be very important [Lov 69]. A satisfactory treatment of exchange effects for composite projectiles is not yet available.

Estimates of their importance can be made by use of a method which has been proposed by Schaefer [Schaf 70] for DWBA analyses of inelastic scattering. Following this method we have simply to add a Gaussian pseudo potential to the effective

$$V_{\text{exch}} = V'_0 \exp(-|\vec{r}-\vec{r}'_\alpha|^2/\mu'_0{}^2)$$

interaction. This pseudopotential depends on the incident energy in order to take account of the nonlocality of the exchange effects. For  $\alpha$ -particles  $\mu'_0$  has the value of 1.31 fm [Schaef 70]. The depth  $V'_0$  is determined by the Fourier transform  $A_{NN}(k_0)$  of the nucleon-nucleon interaction evaluated for a momentum  $k_0$  which is 1/4 the momentum of the incident  $\alpha$ -particles [Sat 71]. The strength  $V'_0$  decreases with increasing energy. Fig. 7 shows the real part of the optical potential calculated for elastic scattering of 166 MeV  $\alpha$ -particles on  $^{208}\text{Pb}$  with and without the exchange pseudo potential ( $V'_0 = -40$  MeV) [Bri 72b]. It may indicate that the influence of the exchange pseudo potential is weak in the active surface region. There the exchange effects (small changes of slope and depth) may be already simulated and absorbed by the phenomenological adjustment of the parameters of the effective interaction. Analyses which introduce explicitly the exchange potential show that this requires a readjustment of the original effective interaction, while in the final results the density distributions are not affected [Bri 72b].

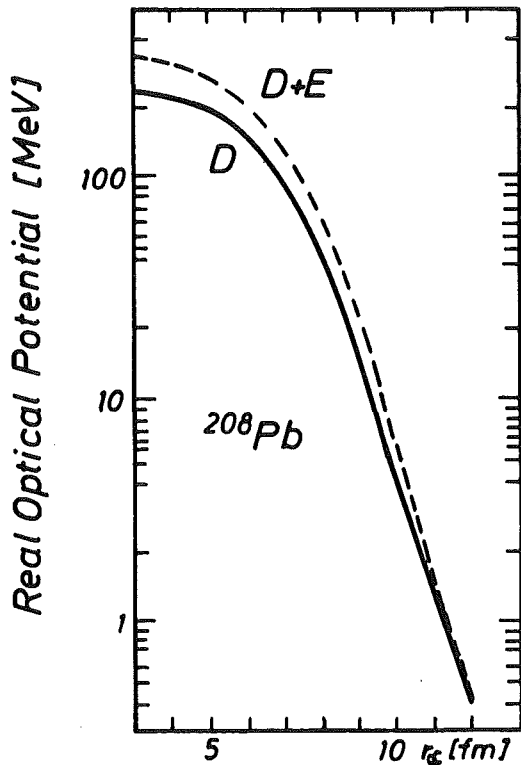


Fig. 8:

Real part of the optical potential calculated for 166 MeV  $\alpha$ -particle scattering from  $^{208}\text{Pb}$  with (D+E) and without (D) exchange pseudo potential

$$V_{\text{exch}} = -40 \exp(-|\vec{r}'_\alpha - \vec{r}|^2 / (1.31)^2)$$

(from Bri 72b)

It is clearly important to explore fully these and other sensitivities before unambiguous information can be deduced concerning nuclear matter distribution, from  $\alpha$ -particle-nuclear elastic scattering. It is, however, encouraging that the folding model gives a good representation of elastic scattering and that the present results for the matter rms radii are entirely consistent with other measurements.

#### IV. Inelastic $\alpha$ -particle scattering

In so called microscopic descriptions of inelastic scattering the coupling potentials  $U_{nn'}$  (form factors) for the nuclear excitation are generated by folding the effective interaction into the transition densities

$$\rho_{nn'}(\vec{r}) = \langle n' | \sum_{i=1}^A \delta(\vec{r} - \vec{r}_i) | n \rangle$$

$$\sum_i^A \int \phi_n^*(\vec{r}_1 \dots \vec{r}_A) \phi_n(\vec{r}_1 \dots \vec{r}_A) d^3r_1 \dots d^3r_{i-1} dr^3_{i+1} \dots d^3r_A$$

$$U_{nn'}(\vec{r}_\alpha) = \int \rho_{nn'}(\vec{r}) V_{\text{eff}}(\vec{r}, \vec{r}_\alpha) d^3r$$

$$= \sum_{LM} F_{LM}(r_\alpha) \cdot Y_{LM}(\hat{r}_\alpha)$$

where  $F_{LM}(r_\alpha)$  are the form factors of the (L,M)-pole-transition. This is obviously in analogy of the folding formula for the elastic scattering. The groundstate nuclear matter distribution  $\rho$  is replaced by the transition density which depends on the nuclear wave functions for the initial and final target nucleus states. In this manner quite successful studies of inelastic nucleon scattering have been carried out [Sat 67, Glen 67, cf. Sat 72a]. In DWBA calculations of this type only the off-diagonal matrix elements are calculated "microscopically" while the diagonal matrix elements are derived from the phenomenological optical potential which is determined by fitting the elastic scattering data and generates the distorted waves. In fact, microscopic treatment of the transition matrix elements ( $n' = n$ ) have been customary before the folding approach of elastic

scattering has become popular.

Similar calculations have been carried out for inelastic  $\alpha$ -particle scattering [Mad 65, Ynt 67, Morg 69, Bern 69, Tat 70, Tat 71, Sat 71, Bim 73, Bri 72a]. However, for lower- $\alpha$ -particle energies the ambiguities - in the sense that different discrete sets of optical potentials fit the elastic scattering - raise some uncertainty over which of these potentials should be used to describe the diagonal matrix elements in a microscopic calculation. It may be also argued that there must be some consistency in the treatment of the diagonal and off-diagonal matrix elements of the effective  $\alpha$ -nucleon interaction. In this spirit more recent DWBA studies [Morg 69, Tat 70, Tat 71, Mac 72, Bim 73, Bim 74] use a microscopic approach to both elastic and inelastic scattering in which the same effective interaction is used to describe both processes. Obviously, especially for coupled channel analyses which handle elastic and inelastic scattering on equal footing this is much more satisfactory.

Fully microscopic calculations construct the transition densities by use of wave functions expressed in a shell model basis. In view of the theoretical uncertainties of the obtained wave functions (single-particle wave function basis, energies and number of configuration states, type of approximation: TDA, RPA ...) such studies of microscopic wave functions may be helpful, provided that the effective interaction is well established. The advantage of  $\alpha$ -particle inelastic scattering over other wave function tests is that it is sensitive to neutron configurations and that for medium high energies the penetrability is sufficient to provide a reasonable test, and yet is not great as to invalidate the results due to possible inaccuracies at small radii. Nevertheless due to the surface localization of  $\alpha$ -particle scattering the role of the tails of the transition densities is emphasized. It is possible that microscopic calculations of the nuclear structure quantities give a good representation of the overall shape but a poor representation of the surface region. In fact the method of folding effective  $\alpha$ -nucleon potentials into microscopic nucleon densities, although satisfactory in some cases, has not met with the same success as for the elastic scattering. Most likely this is not caused by a breakdown of the effective interaction but rather by the incomplete description of collective

excitations by means of individual shell model configurations [Bern 69].

Recently, in regard of the critique of the usual collective model description of inelastic scattering [Ed 71, Ter 73] and in order to investigate the relation between nuclear matter and nuclear potential deformations, in several exploratory calculation [Ed 71, Ra 72, Sat 72b] and analyses of experimental ( $\alpha, \alpha'$ )-results [Re 73a, Re 74a, Re 74b, Mac 73, Mac 74, Gi 74] the transition densities has been derived from phenomenologically deformed matter distributions. Such a semi-microscopic approach which is a simple and natural generalization of the corresponding procedure for the elastic  $\alpha$ -particle scattering proves to be relevant to higher energy  $\alpha$ -particles due the increased sensitivity on shape and size parameters and due to the reduced importance of the exchange effects. Of course we may regard this undertaking as a trial, and on this trial we will use again a comparison to electromagnetic results as a guide.

We illustrate this approach with recent results of 104 MeV  $\alpha$ -particle scattering on  $^{56}\text{Fe}$ . In essential, the procedure consists in a application of the collective model - whatever the specific form may be - to the density distribution  $\rho$  of the integrand of the folding formula rather than to the optical potential. The derivation of the coupling potentials is straightforward and indicated in fig. 9a for a vibrational model of higher orders, as example. Fig. 9b shows the formfactors for the rotational model. For further technical details we refer to original papers, especially to the appendix of the paper of Rebel et al. [Re 74a].

We start with a rotational model description of  $^{56}\text{Fe}(\alpha, \alpha')^{56}\text{Fe}$ .

The level positions and E2 properties of  $^{56}\text{Fe}$  are characteristic of an almost pure prolate rotator. The experimental  $B(E2; 0^+ \rightarrow 2^+_1)$ ,  $B(E2; 2^+_1 \rightarrow 4^+_1)$  and  $Q_{2+}$ -values [Les 72] correspond to intrinsic quadrupole moments of  $98 \pm 1$ ,  $99 \pm 20$  and  $87 \pm 20$  efm<sup>2</sup>, respectively, derived on the basis of a symmetric rotator model. But they are also consistent with  $Q_0 = 102$  efm<sup>2</sup> and  $\gamma = 20^\circ$  in the asymmetric rotator model. Davydov and Chaban [Dav 60] explained the level scheme of  $^{56}\text{Fe}$  in the framework of an asymmetric rotator model with  $\beta$ -vibrations resulting in  $\gamma = 17^\circ$  and a softness  $\mu = 0.61$ .

Extended optical potential

Folding procedure

$$U_R(\vec{r}_\alpha, \xi) \rightarrow \sum_{LM} U_{LM}^R(r_\alpha, \xi) Y_{LM}(\theta_\alpha, \phi_\alpha) \leftarrow \int \rho(\vec{r}, \xi) V_{eff}^{N\alpha}(\vec{r}, \vec{r}_\alpha) d^3r$$

$$V_{eff}^{N\alpha}(r, r_\alpha) = \sum_{\lambda\mu} v_{\lambda\mu}(r, r_\alpha) Y_{\lambda\mu}^*(\theta, \phi) Y_{\lambda\mu}(\theta_\alpha, \phi_\alpha)$$

$$\rho(r, \theta, \phi) = \sum_{lm} \rho_{lm}(r, \xi) Y_{lm}(\theta, \phi)$$

$$U_{LM}^R(r_\alpha, \xi) = 4\pi \int r^2 dr \rho_{lm}(r, \xi) v_{lm}(r, r_\alpha)$$

Example: Collective surface vibrations

$$R = R_0 (1 + \sum_{lm} \alpha_{lm} Y_{lm})$$

$$U_R(r_\alpha - R(\theta_\alpha, \phi_\alpha)) =$$

$$u^{(0)}(r_\alpha) + \sum_{lm} \sum_t [u^{(t)}(r_\alpha) \alpha_{lm}^{(t)}] Y_{lm}(\theta_\alpha, \phi_\alpha)$$

$$u^{(t)} = \frac{R_0^t}{t!} \frac{\delta^t U}{\delta R^t}$$

$$c = c_0 (1 + \sum_{lm} \alpha_{lm} Y_{lm})$$

$$\rho(r - c(\theta, \phi)) =$$

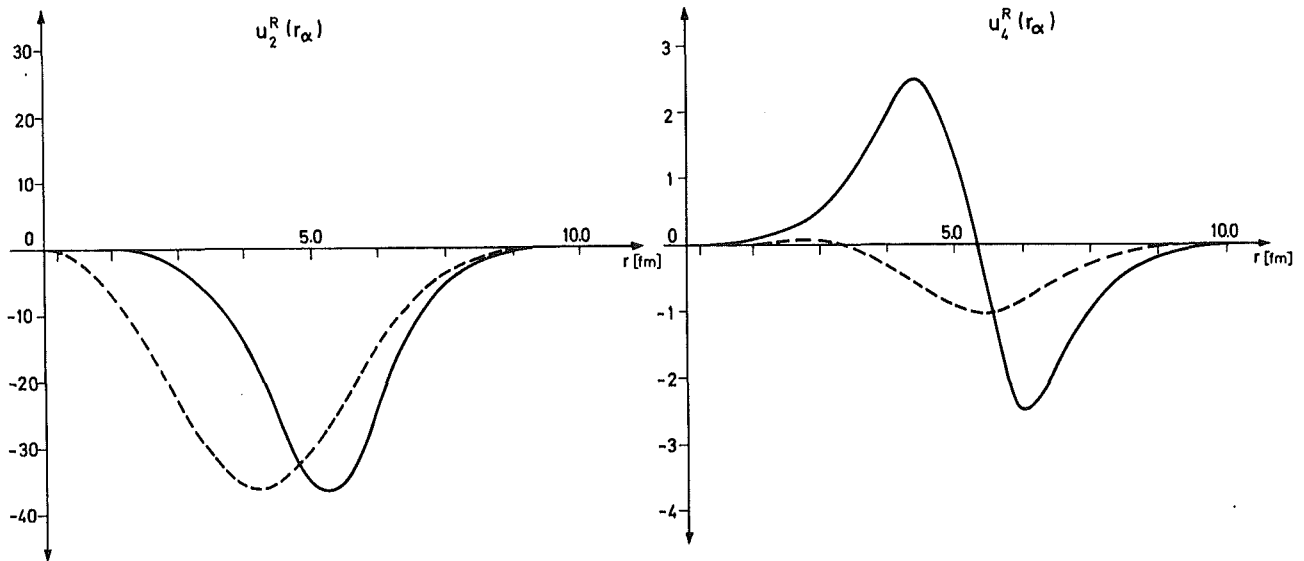
$$\rho^{(0)}(r) + \sum_{lm} \sum_t [\rho^{(t)}(r) \alpha_{lm}^{(t)}] Y_{lm}(\theta, \phi)$$

$$\rho^{(t)}(r) = \frac{c_0^t}{t!} \frac{\delta^t \rho}{\delta c^t}$$

$$\alpha_{lm}^{(1)} = \alpha_{lm}$$

$$\alpha_{lm}^{(t)} = \sum \sqrt{\frac{2(l'+1)(2l'+1)}{2l'+1}} \langle l' l' 0 0 | l 0 \rangle [\alpha_{l'}^{(t-1)} \otimes \alpha_{l''}]_{lm}$$

Fig. 9a: Application of the collective model in the framework of the extended optical model and of the folding model



Comparison of the radial formfactors for a permanently deformed potential:  $U_R(\vec{r}_\alpha) = \sum_{L=0}^L U_L^R(r_\alpha) \cdot D_{MO}^L Y_L^M(\hat{r}_\alpha)$  for the extended optical model (—) and the folding model (---) using a deformed density distribution of  $^{56}\text{Fe}$  (Parameter values taken from Gils et al 1974).

Fig. 9b: Comparison of the form factors derived on the basis of the rotational model in the framework of the extended optical model and of the folding model

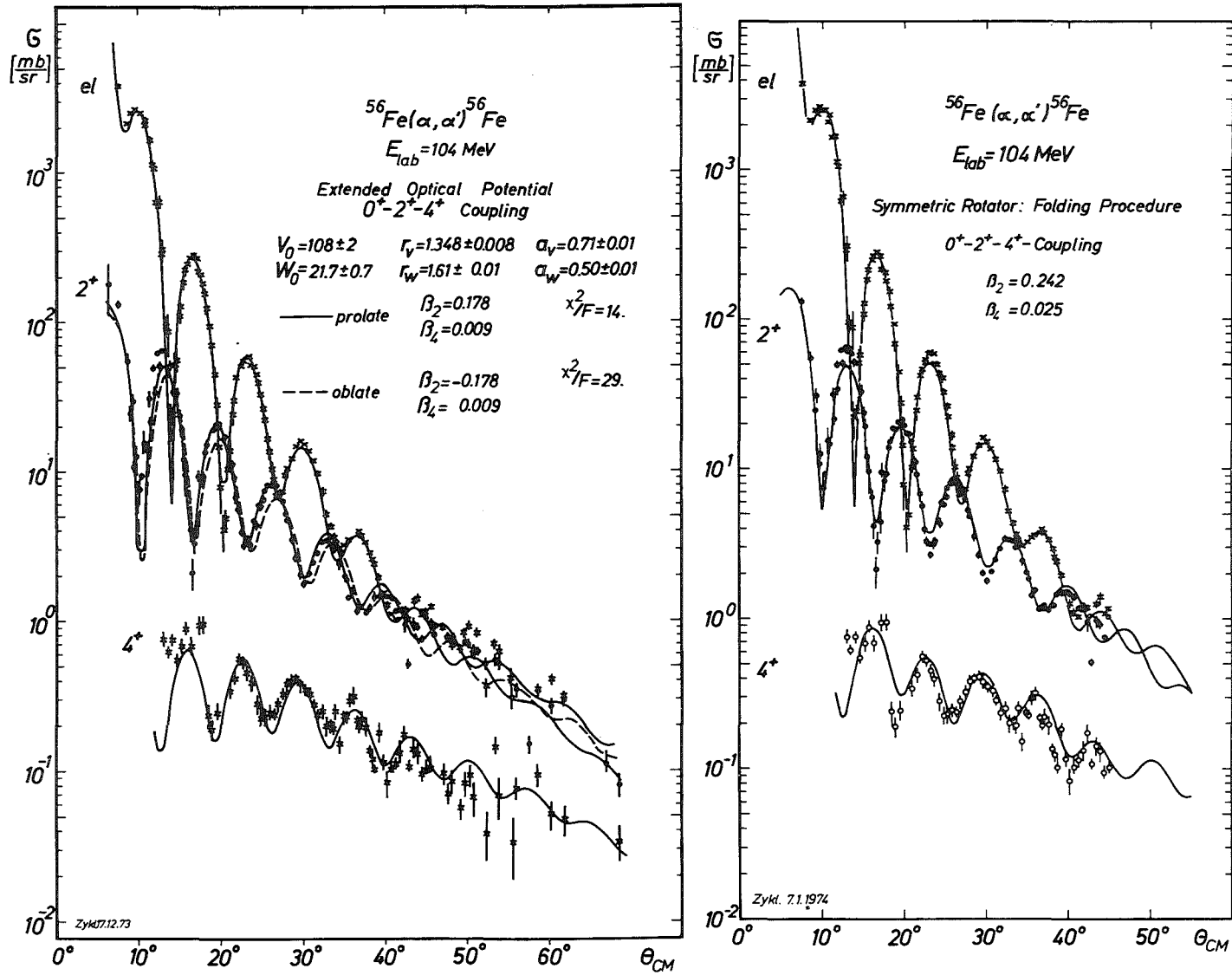


Fig. 10: Coupled channel analysis of the scattering of 104 MeV  $\alpha$ -particles from  $^{56}\text{Fe}$  on the basis of the rotational model [Gi 74]

Fig. 10 compares the results of the extended optical potential of Saxon-Woods form (parameters taken from a coupled channel calculation fit of the cross sections) to those of the folding model using a deformed nuclear density distribution of fermi type. Of course, the main effect of the folding is a correction due to the finite size of the probe represented by the finite range of  $V_{\text{eff}}$ , and this is reflected by different values of the deformation parameters.

Hendrie [Hen 73] has worked out a correction procedure based on a pure geometrical consideration assuming a spherical projectile interacting with a deformed nucleus only at their mutual sharply defined edges. With a  $\alpha$ -particle size of  $\Delta=1.6$  fm and a sharp edge size of  $1.2 \cdot A^{1/3}$  for  $^{56}\text{Fe}$  the value of  $\beta_2=0.24$  would correspond to the potential deformation  $\beta_2^{\text{Pot}} \approx 0.18$ .

The value of  $\beta_2=0.24$  of the underlying fermi distribution corresponds to an intrinsic quadrupole moment which is in excellent agreement with the electromagnetic results. The prolate-oblate effects are significant and give evidence for prolate deformation of  $^{56}\text{Fe}$  - in agreement with Coulomb excitation [Les 72].

Tab. 2 compiles some results for nuclei of the 1f-2p-shell and compares with results of electron scattering and Coulomb excitation. Of course, the  $\alpha$ -particle scattering results are model-dependent. But in the framework of these specific collective models suggested by spectroscopic findings  $\alpha$ -particle scattering provides detailed information, for example, on the asymmetry of the deformation ( $^{48}\text{Ti}$ ,  $^{56}\text{Fe}$ ) or on hexadecapole deformations. The table may demonstrate the general agreement of the deformed folding model with electromagnetic results. This is an empirical result remarkable in regard of the considerable uncertainties of such an approach.

Concerning the model dependence of these and similar results, the collective model interpretation may not be taken too literally if we restrict our considerations to the outermost surface region and higher order processes do not contribute significantly. In every reasonable model the transition densities  $\rho_{nn'}$  have a similar fall off as the collective model form factors. The "deformation parameters" provide the normalisation. This aspect is underlying to Bernstein's procedure of extraction "model independent" isoscalar transition rates [Bern 69]. But we cannot follow the logic using the extended optical potential for analysing the data and assuming the vibrational amplitude  $\beta \cdot R$  is the same for both the nucleus and the optical potential [Bl 60].

Nuclide	46 Ti	48 Ti	50 Ti	56 Fe		
$\langle r^2 \rangle^{1/2}$ [fm]	3.64±0.15	3.56±0.04	3.60±0.07	3.75±0.06	3.82±0.06	$\alpha$
$B(E2, 0^+ \rightarrow 2^+)$ [e <sup>2</sup> fm <sup>4</sup> ]	874±56	763±40	280±26	1009±62	1047±60	
$Q_{2^+}$ [efm <sup>2</sup> ]	-27±1	-19±1	—	-29±1	-29±1	
$\gamma$	—	≈ 24°	—	—	≈ 19°	
Analysis	Symmetric Rotator	Triaxial Rotator	Anharmonic Vibrator	Symmetric Rotator	Triaxial Rotator	
$\langle r^2 \rangle^{1/2}$ [fm]	3.55±0.04			3.74±0.07		e
$B(E2, 0^+ \rightarrow 2^+)$ [e <sup>2</sup> fm <sup>4</sup> ]	970±70	690±60	330±30	970±20		Coulomb-E
$Q_{2^+}$ [efm <sup>2</sup> ]	-19±10	-13.5±8.8	-2±9	-24.9±5.8		

Tab. 2: Folding model results for the scattering of 104 MeV  $\alpha$ -particles from 1f-2p shell nuclei and comparison to electromagnetic results [Re 74a, Gi 74, Re 74c]

A further illustration is given by the hexadecapole deformation studies for 2s-1d shell nuclei [Re 74a]. A puzzling discrepancy had become apparent between (p,p') and ( $\alpha,\alpha'$ ) results in that (p,p') scattering finds appreciably larger values of hexadecapole deformation.

In Tab. 3 for <sup>20</sup>Ne and <sup>28</sup>Si results of various analyses are compiled and suggests that the folding model may be able to remove such discrepancies. Detailed studies of the nuclear deformation of <sup>20</sup>Ne, <sup>24</sup>Mg and <sup>28</sup>Si using folding models have been carried out by Mackintosh et al. [Mac 73, Mac 74] on the basis of the experimental results at  $E_\alpha = 104$  MeV. An interesting aspect comes from the studies of the sensitivity to various ways of deforming the nucleus.

The standard prescription introducing the parametrization of the half density radius  $c_m$  is certainly not the most general means of deforming a nucleus and may be unphysical in some respects [Tas 73]. For a deformed distribution of the form

$$\rho(\vec{r}) = \rho(r - c_m(\Omega'))$$

with  $c_m(\Omega') = c_o(1 + \sum \beta_\ell Y_{\ell 0}(\Omega'))$

the equi-density-surfaces of  $\rho$  are given by

$$r = r_o + c_o \sum \beta_\ell Y_{\ell 0}(\Omega')$$

The deformation of the outer part of the nucleus seems to be smaller than of the inner part, and this may induce effects dependent on the energy and type of the projectile. Satchler [Sat 92b] and Tassie [Tas 73] propose more general ways of deforming the density distribution, e.g. by introducing

$$\vec{r} = r_o (1 + \sum \beta_\ell Y_{\ell 0}(\Omega'))$$

as equi-density surfaces.

	$\langle r^2 \rangle^{1/2}$ [fm]	$\beta_2$	$\beta_4$	$Q_o$ [efm <sup>2</sup> ]	Method
<sup>20</sup> Ne	2.91	+0.40	+0.19	60(7)	B(E2,0 <sup>+</sup> →2 <sup>+</sup> )
		+0.47	+0.28(5)	+80(17)	Q <sub>2</sub>
	2.99	+0.35(1)	+0.11(1)	+58(3)	(e,e')
		+0.42(1)	+0.29(1)	+53	(p,p')
<sup>28</sup> Si	3.14	-0.39	+0.10	-64(3)	(α,α')
		(-)0.34	+0.25(8)	-54	(α,α') Fold.
		-0.32(1)	+0.08(1)	-52	B(E2,0 <sup>+</sup> →2 <sup>+</sup> )
	3.04	-0.39(1)	+0.27(3)	-57	Q <sub>2</sub>
					(e,e')
					(p,p')

The deformation of <sup>20</sup>Ne and <sup>28</sup>Si from different methods

Tab. 3: Comparison of various deformation studies for <sup>20</sup>Ne and <sup>28</sup>Si

This is of more than academic interest since electron scattering analyses take prescriptions of more general types ("uniform strain") prescription or even the "Tassie model" [Tas 56] rather than a surface deformation. Yet, people usually compare the  $\beta_\ell$  without regard on this. The calculations of Mackintosh and Tassie [Mac 74] result in surprisingly stable values of the quadrupole moment and also determine the hexadecapole moment fairly unambiguously for

the different manners of deforming the nucleus.

The collective models used hitherto are relatively simple and limiting cases for the collective behaviour of nuclei. In particular, nuclei of the 1f-2p shell exhibit features characteristic of soft nuclei. The properties of the low-lying levels indicate collective features intermediate between harmonic vibrations and rigid rotations [Cli 71]. In such transitional cases we need a more general and flexible description - generalized collective model - as formulated e.g. by Gneuß and Greiner [Gneu 71]. As for any other collective Hamiltonian we have to determine several mass- and stiffness parameters which, in principle, may be related to a microscopic description of the collective motion. We used, however, a rather phenomenological procedure in determining these parameters by fitting the experimental level schemes and  $B(E2; 0^+ \rightarrow 2^+)$  transition probabilities. Such a procedure has been proved to be very successful in a range of cases [Re 73b, Hab 74]. The collective behaviour of the nuclei is displayed by their so-called collective energy surfaces. They represent the potential energy of the nuclei as function of the shape parameters. With restriction to quadrupole deformations all possible shapes can be described by the two well-known deformation and asymmetry parameters  $\beta$  and  $\gamma$ . Fig. 11 shows the collective energy surfaces of  $^{48}\text{Ti}$  and  $^{56}\text{Fe}$  given as contour maps on the  $\beta$ - $\gamma$ -plane. Symmetry properties confine the considerations on a sector  $0^\circ < \gamma < 60^\circ$ . In this sector the potential energy surfaces and the collective wave functions are defined. The shadowed contours indicate the level of the ground states and the range of the zero-point-oscillations. This may be taken as a measure of the softness of these nuclei:  $^{48}\text{Ti}$ , a  $\beta$ -soft nucleus with asymmetric deformation,  $^{56}\text{Fe}$  some what more complicated exhibiting a second minimum, yet in the range of the zero-point oscillations.

In view of the considerable importance of the collective energy surfaces with regard on heavy ion scattering, nuclear fission etc. it is certainly interesting to check such calculations by  $\alpha$ -particle scattering.

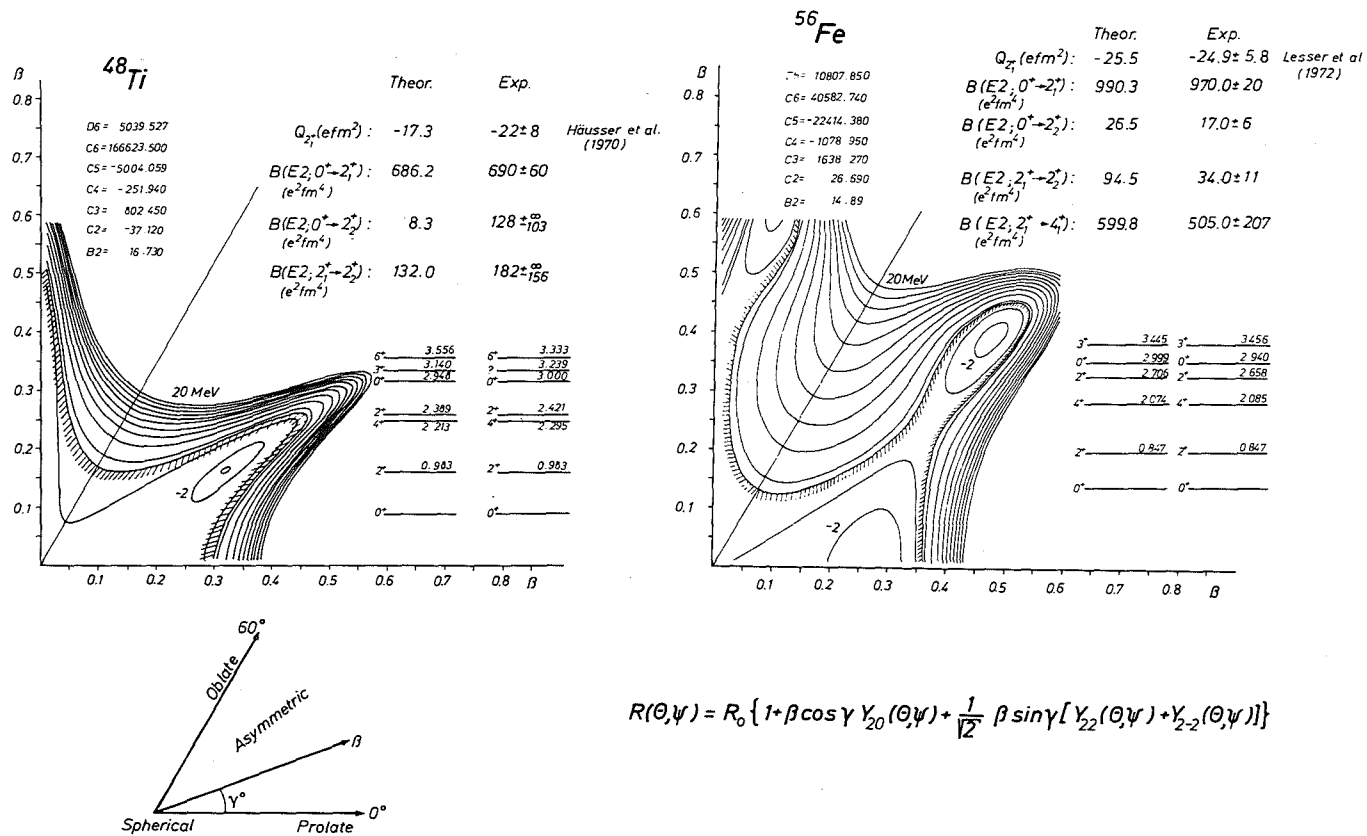


Fig. 11: Collective energy surfaces of  $^{48}\text{Ti}$  and  $^{56}\text{Fe}$  resulting from an analysis of level spectra and E2 properties in the framework of the model of Gneuß and Greiner [Re 74b]

Formally, the generalized collective model is an anharmonic vibrational model of high order (as formulated \*) in fig. 9a). This implies that

1. matrix elements of second and higher orders of the collective coordinates contribute significantly.
2. the values of the matrix elements are strongly dependent on the connected states in rather complex relations.

The matrix elements for the  $(\alpha, \alpha')$ -scattering calculations are obtained directly by the solutions of the collective Hamilton. The radial behaviour of the density distribution can be taken from elastic or electron scattering, and as also the effective interaction is fixed, we have not to adjust any parameters.

The sensitivity of the scattering cross sections to higher order matrix elements is shown in fig. 12 and demonstrates that 100 MeV  $\alpha$ -particles are able to "see" the rather complicated nuclear shapes represented by the collective energy surfaces in fig. 11. In fig. 13 we demonstrate the excellent agreement of  $\alpha$ -particle scattering with the generalized collective model. The imperfectness for the  $2_2^+$ -cross section may indicate the presence of an unknown admixture to the  $2_2^+$  amplitude (e.g. coupling of two quasiparticle states neglected in the generalized collective model). This assumption is not unreasonable for a level of 2.7 MeV above the ground state. In view of the extreme sensitivity of the  $\alpha$ -particle cross sections to such additional components there is no serious objection against the generalized collective model description of the low lying states.

We may conclude that the generalized collective model proves to be an excellent basis for a unified description of level scheme, E2-properties and  $\alpha$ -particle scattering. Scattering of  $\alpha$ -particles is sensitive enough to reveal more complicated collective features and to draw attention to necessary improvements of the current structure models.

---

\*) Requiring volume conservation and considering terms of higher orders a monopole term  $\alpha_{00}$  has to be introduced into the expansion of the nuclear radius and induces additional coupling terms not given in fig. 9a [Re 74b]

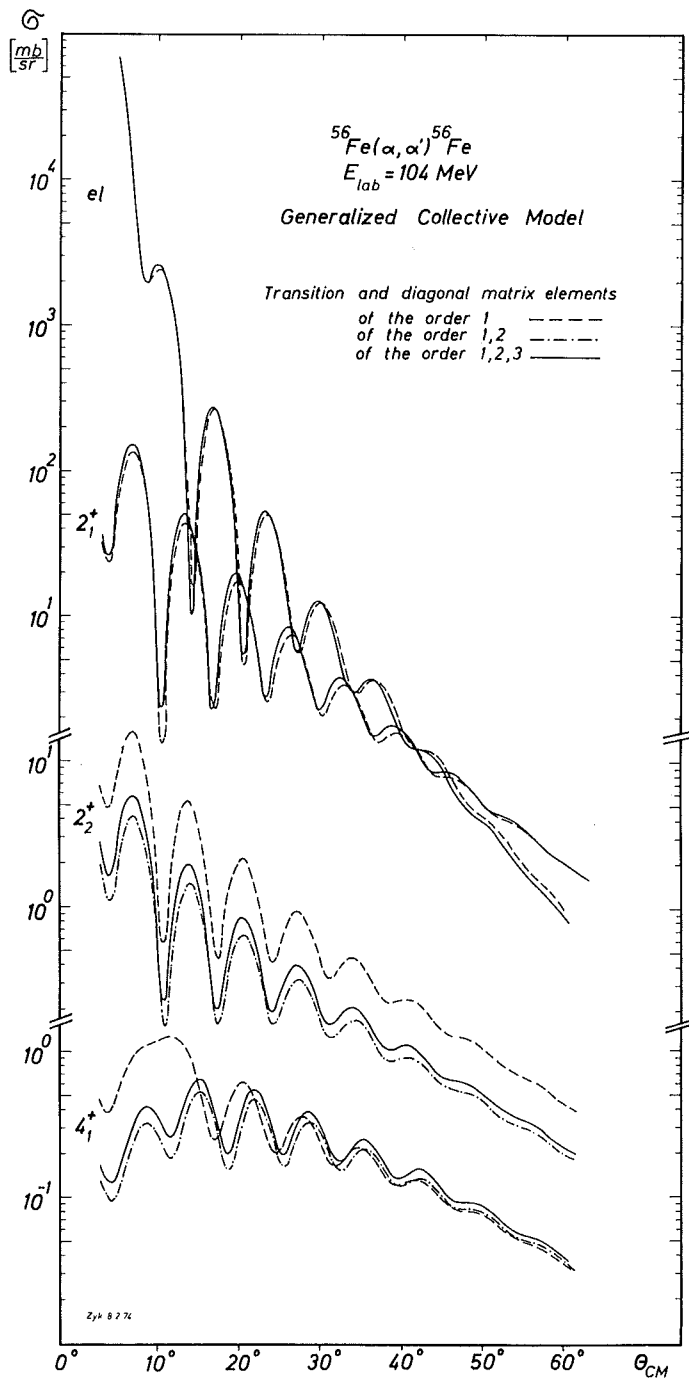


Fig 12: Generalized collective model description of  $^{56}\text{Fe}(\alpha, \alpha')^{56}\text{Fe}$   
Theoretical cross sections calculated by including  
different orders of transition matrix elements

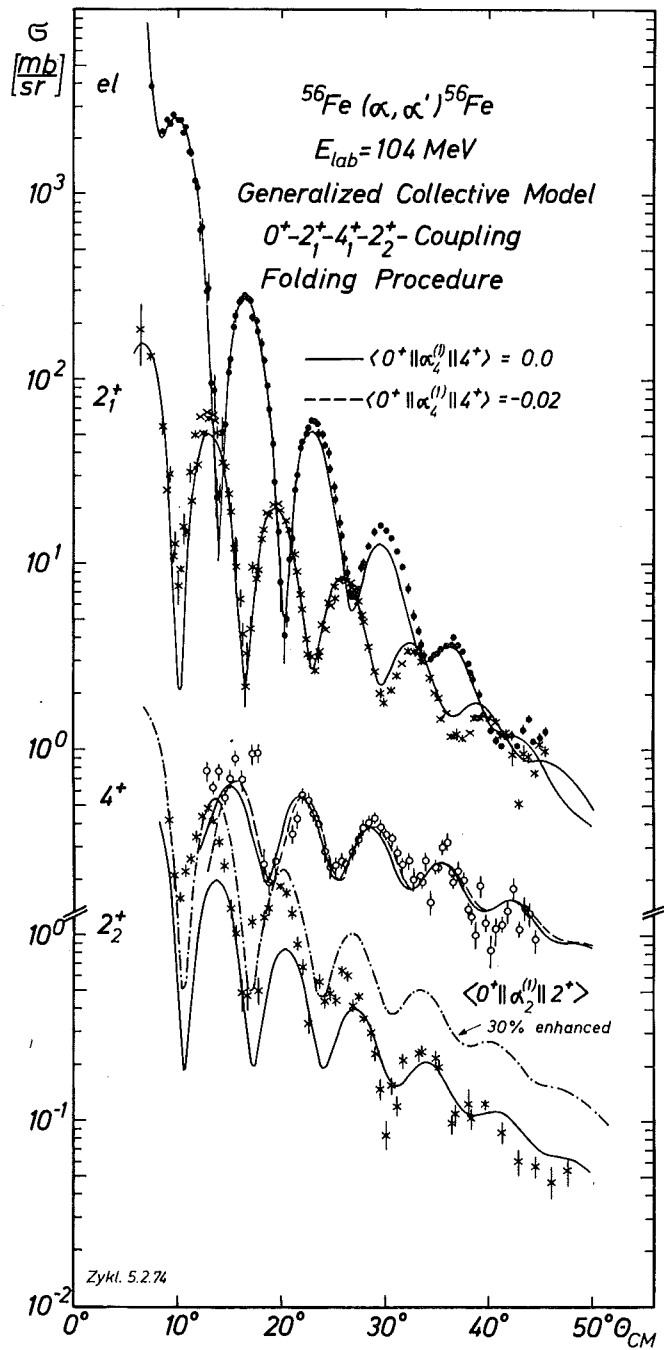


Fig. 13: Generalized collective model description of  $^{56}\text{Fe}(\alpha, \alpha')^{56}\text{Fe}$  at  $E_\alpha = 104 \text{ MeV}$ : Coupled channel predictions and experimental cross sections [Re 74b]

## V. Concluding remarks

This review establishes the considerable success of the folding model of  $\alpha$ -particle scattering as description of elastic and inelastic scattering from collective states, in particular at higher bombarding energies. The results concerning the nuclear density distributions are in excellent agreement with the information obtained by other methods, e.g. electron scattering, and we have no reason to distrust in results providing new information. The facts reveal empirical evidence for the relevance of the folding approach. Nevertheless in the present stage of our knowledge and understanding there are various questions which require further studies and suggest refinements:

### 1. Effective interaction:

Although we may follow the statement of Batty et al. [Batt 71b] that the effective  $\alpha$ -nucleon interaction is well determined, it is far from evident that a single local, density independent interaction can simultaneously give a satisfactory representation of both the diagonal and non-diagonal parts of the  $\alpha$ -nucleus effective interaction.

Based on more or less convincing arguments different attitudes have been developed, in deriving the currently used local effective interactions. Though different they prove to be successful in the considered cases where they have been applied. However, it is by no means clear how they work in a different case and which is the most reliable type in a specific situation. In particular, there is a lack of a consistent investigation with emphasis to the energy dependence in elastic and inelastic scattering.

### 2. Exchange effects:

Exchange effects may be of minor importance at higher energies and for forward scattering. But there is no reliably quantitative estimate of these effects which influence inelastic scattering to a larger extent than elastic scattering. Some exploratory calculations using a pseudo potential seem to indicate the influence increasing with the transition multipolarity [Sat 72b, Bern 72]. But it may be possible to absorb

the effects - at least for the diffraction region of the cross sections - by the adjustment of the phenomenological interaction.\*) We feel there is a great uncertainty of the folding approach.

### 3. Imaginary part of the potentials:

As we have no reliable microscopic description of the imaginary part we use a phenomenological shape. The role of the imaginary part and its sensitivity to the specific form of the real effective interaction is not explored.

### 4. Model dependence:

Calculations using different ways of deforming the nuclear density distributions [Mac 74] or different parametrizations of a surface deformation [Re 74a] show that the rms-radius and the multipole moments are better determined by the experimental data than the model parameters. This suggests to seek for a more model independent formulation as achieved for electron scattering [Le 69, Fri 72]. The modern approach is to concentrate on the moments of the distributions rather than on a single functional form.

Investigations of these and further questions will refine and consolidate the folding model. The presented encouraging results from the present stage let expect relevant information about the nuclear density distributions, about surface, size and shape of the nuclei.

---

\*) For larger scattering angles, beyond the diffraction region we observe significant deviations of the folding model predictions in that the experimental cross sections decrease less rapidly with angle. This feature may be a consequence of exchange effects and is reproduced by the shorter range of the exchange pseudo-potential.

### Acknowledgement

These lectures are intended to be an experimentalist's view of the sense and the current situation of the folding model of  $\alpha$ -particle scattering.

It is a pleasure to acknowledge illuminating conversations on the subject of  $\alpha$ -particle scattering and the folding model with H.J. Gils, P.E. Hodgson, G.W. Greenlees, G.H. Rawitscher, G.R. Satchler, G. Schatz, P.P. Singh and G.W. Schweimer.

## References

- Als 66 J. Alster, D.C. Streve and R.J. Peterson;  
Phys. Rev. 144 (1966) 999
- Asc 71 R.J. Ascutto, N.K. Glendenning and Bent Sørensen;  
Nucl. Phys. A170 (1971) 65; Phys. L. 47B (1973) 332
- Au 65 N. Austern and J.S. Blair, Ann. Phys. 33 (1965) 15
- Bach 72 D. Bachelier, M. Bernas, J.L. Boyard, H.L. Harney,  
J.C. Jourdain, P. Radvanyi and M. Roy-Stephan;  
Nucl. Phys. A195 (1972) 361
- Bar 74 A.R. Barnett and J.S. Lilley; Phys. Rev. C9 (1974) 2010
- Batt 71a C.J. Batty and E. Friedman; Phys. L. 34B (1971) 7
- Batt 71b C.J. Batty, E. Friedman and D.F. Jackson;  
Nucl. Phys. A175 (1971) 1
- Bern 69 A. Bernstein; Advances in nuclear physics, vol. 3  
ed. M. Baranger and E. Vogt (1969) p. 325
- Bern 71 A.M. Bernstein and W.A. Seidler; Phys. L. 34B (1971) 569
- Bern 72 A.M. Bernstein and W.A. Seidler; Phys. L. 39B (1972) 583
- Bim 73 L. Bimbot, B. Tatischeff, I. Brissaud, Y. Le Bornec,  
N. Frascaria and A. Willis; Nucl. Phys. A210 (1973) 397
- Bim 74 L. Bimbot, I. Brissaud, Y. Le Bornec, B. Tatischeff,  
N. Willis and M. Soyeur; Phys. L. B49 (1974) 443
- Bri 72a I. Brissaud, B. Tatischeff, L. Bimbot, V. Comparat,  
A. Willis and M.K. Brussel; Phys. Rev. C6 (1972) 595
- Bri 72b I. Brissaud, Y. Le Bornec, B. Tatischeff, L. Bimbot,  
M.K. Brussel et. G. Duhamel; Nucl. Phys. A191 (1972) 145
- Bl 54 J.S. Blair; Phys. Rev. 95 (1954) 1218
- Bl 60 J.S. Blair; Proceedings of the Int. Conf. on Nuclear  
Structure, Kingston, Canada (1960)
- Bud 70 A. Budzanowski, A. Dudek, K. Grotowski and  
A. Strzalkowski; Phys. L. 32B (1970) 431
- Bud 74 Proceedings of the 1st Louvain-Cracow Seminar,  
Cracow 1974, Rep. No. 870/PL, ed. by A. Budzanowski
- Cli 71 D. Cline; Proc. Colloq. on intermediate nuclei, Orsay,  
France, 1971, UR-NSRL 59 (1972)
- Dav 60 A.S. Davydow and A.A. Chaban; Nucl. Phys. 20 (1960) 499
- Du 68 H.H. Duhm; Nucl. Phys. A118 (1968) 563
- Ed 71 V.R.W. Edwards and B.C. Sinha; Phys. L. 37B (1971) 225

- Eis 61 R.M. Eisberg and C.E. Porter; Rev. Mod. Phys. 33  
(1961) 190
- Elt 64 L.R.B. Elton and A. Swift; Proc. Phys. Soc. 84 (1964)125
- Fe 70 B. Fernandez and J.S. Blair; Phys. Rev. C1 (1970) 523
- Fes 58 H. Feshbach; Ann. Phys. N.Y. 5 (1958) 357
- Fic 70 J.R. Ficenec, W.P. Trower, J. Heisenberg and I. Sick;  
Phys. L. 32B (1970) 460
- For 59 K.W. Ford and J.A. Wheeler; Ann. Phys. 7 (1959) 259;  
ibid 7 (1959)287
- Fri 72 F. Friedrich and F. Lenz; Nucl. Phys. A183 (1972) 523
- Gi 74 H.J. Gils, H. Rebel and A. Ciocanel; Rev. Roum. de Phys.  
in press
- Glen 66 N.K. Glendenning and M. Veneroni; Phys. Rev. 144 (1966)839
- Glen 67 N.K. Glendenning; Proc. Int. School of Physics  
"Enrico Fermi" course 40, 1967 ed. M. Jean (Academic  
Press, N.Y. 1969)
- Gneu 71 G. Gneuß and W. Greiner; Nucl. Phys. A71 (1971) 449
- Gol 72 D.A. Goldberg and S.M. Smith; Phys. Rev. L. 29 (1972) 500
- Gol 73 D.A. Goldberg, S.M. Smith, H.G. Pugh, P.G. Roos and  
N.S. Wall; Phys. Rev. C7 (1973) 1938
- Gol 74 D.A. Goldberg, S.M. Smith and G.F. Burdzik;  
University of Maryland, Department of Physics and  
Astronomy, Tech. Rep. No. 74-107 (1974)
- Gon 71 V.Yu Gonchar and A.V. Yushkov; Bull. Acad. of Sci.,  
USSR, Phys. Ser. 35 (1971) 558
- Green 68 G.W. Greenlees, G.J. Pyle and Y.C. Tang; Phys. Rev. 171  
(1968) 1115
- Hab 74 D. Habs, H. Klewe-Nebenius, K. Wisshak, R. Löhken,  
G. Nowicki and H. Rebel; Z. Phys. 267 (1974) 149
- Haus 69 G. Hauser, R. Löhken, H. Rebel, G. Schatz, G.W. Schweimer  
and J. Specht; Nucl. Phys. A128 (1969) 81
- Hen 73 D.L. Hendrie; Phys. Rev. L31 (1973) 478
- In 67 E.V. Inopin and A.V. Shebeko; JETP (Sov. Phys.) 24  
(1967) 1189
- Jack 68 D.F. Jackson and C.G. Morgan; Phys. Rev. 175 (1968) 1402
- Jack 69a D.F. Jackson and V.K. Kumbhavi; Phys. Rev. 178 (1969)1626
- Jack 69b D.F. Jackson; Nucl. Phys. A123 (1969) 273
- Jack 74 D.F. Jackson; Rep. Prog. Phys. 37 (1974) 55

- Le 69 F. Lenz; Z. Phys. 222 (1969) 491
- Lern 72 G.M. Lerner, J.C. Hubert, L.L. Rutledge Jr. and  
A.M. Bernstein; Phys. Rev. C6 (1972) 1254
- Les 72 P.M.S. Lesser, D. Cline, P. Goode and R.N. Horoshko;  
Nucl. Phys. A190 (1972) 597
- Lil 71 J.S. Lilley; Phys. Rev. C3 (1971) 2229
- Lov 69 W.G. Love, L.W. Owen, R.M. Drisko, G.R. Satchler,  
R. Stafford, R.J. Phillipott and W.T. Pinkston;  
Phys. L. 29B (1969) 478
- Mac 72 R.S. Mackintosh; Nucl. Phys. A198 (1972) 343
- Mac 73 R.S. Mackintosh; Nucl. Phys. A210 (1973) 245
- Mac 74 R.S. Mackintosh and L.J. Tassie; Nucl. Phys. A222 (1974)  
187
- Mad 65 V.A. Madsen and W. Tobocman; Phys. Rev. 139 (1965) B864
- Madl 74 D.G. Madland, P. Schwandt, W.T. Sloan, P. Shapiro,  
P.P. Singh; preprint 1974 - P.P. Singh, private  
communication
- Mail 72 P. Mailandt, J.S. Lilley and G.W. Greenlees;  
Phys. Rev. L. 28 (1972) 1075
- Mail 73 P. Mailandt, J.S. Lilley and G.W. Greenlees;  
Phys. Rev. C8 (1973) 2189
- Morg 69 C.G. Morgan and D.F. Jackson; Phys. Rev. 188 (1969) 1758
- My 73 W.D. Myers; Nucl. Phys. A204 (1973) 465
- Pu 74 L.W. Put and A.M.J. Paans; Phys. L. 49B (1974) 266
- Ra 71 G.M. Rawitcher and R.A. Spicuzza; Phys. L. 37B (1971) 221
- Ray 71 J. Raynal; Report DPh-T/71-48, Saclay (1971)
- Re 72a H. Rebel; Nucl. Phys. A180 (1972) 332
- Re 72b H. Rebel, G.W. Schweimer, G. Schatz, J. Specht,  
R. Löhken, G. Hauser, D. Habs and H. Klewe-Nebenius;  
Nucl. Phys. A182 (1972) 145
- Re 72c H. Rebel, R. Löhken, G.W. Schweimer, G. Schatz and  
G. Hauser; Z. Physik 256 (1972) 258
- Re 73a H. Rebel and G.W. Schweimer; Z. Physik 262 (1973) 59
- Re 73b H. Rebel and D. Habs; Phys. Rev. C8 (1973) 1391
- Re 74a H. Rebel, G. Hauser, G.W. Schweimer, G. Nowicki,  
W. Wiesner and D. Hartmann; Nucl. Phys. A218 (1973) 13
- Re 74b H. Rebel, G.W. Schweimer, D. Habs and H.J. Gils;  
Nucl. Phys. A225 (1974) 457
- Re 74c H. Rebel; unpublished material and results of the  
Karlsruhe group

Reed 68 M. Reed; Thesis, University of California, UCRL-18414  
 (1968)

Sat 67 G.R. Satchler; Nucl. Phys. A95 (1967) 1

Sat 68 G.R. Satchler, L.W. Owen, A.J. Elwyn, G.L. Morgan  
 and R.L. Walter; Nucl. Phys. A112 (1968) 1

Sat 71 G.R. Satchler; Nuclei and Particles 2 (1971) 265

Sat 72a G.R. Satchler; Comm. Nucl. Particles Phys. V (1972) 39

Sat 72b G.R. Satchler; Phys. L. 39B (1972) 495; private  
 communications

Schaefer 70 R. Schaeffer; Nucl. Phys. A158 (1970) 321

Schwa 72 D. Schwalm, A. Bamberger, P.G. Bizzeti, B. Povh,  
 G.A.P. Engelbertink, J.W. Olness and E.K. Warburton;  
 Nucl. Phys. A192 (1972) 449

Schwei 73 G.W. Schweimer and J. Raynal; preprint (1973) and  
 private communications

Sin 69 P.P. Singh, R.E. Malmin, M. High and D.W. Devins;  
 Phys. Rev. L23 (1969) 1124

Sin 72 P.P. Singh and P. Schwandt; Phys. L. 42B (1972) 181

Sin 74 P.P. Singh; private communication (1974)

Smi 73 S.M. Smith, G. Tibell, A.A. Cowley, D.A. Goldberg,  
 H.G. Pugh, W. Reichart and N.S. Wall; Nucl. Phys. A207  
 (1973) 273

Ta 65 T. Tamura; Rev. Mod. Phys. 37 (1965) 679

Ta 67 T. Tamura; ORNL-Report No. 4152 (1967);  
 H. Rebel and G.W. Schweimer, KFK-Report No. 1333 (1971)

Tat 70 B. Tatischeff and I. Brissaud; Nucl. Phys. A155 (1970) 89

Tat 71 B. Tatischeff, L. Bimbot, I. Brissaud, V. Comparat,  
 A. Willis and M.K. Brussel; Phys. Rev. C4 (1971) 494

Tat 72 B. Tatischeff, I. Brissaud and L. Bimbot; Phys. Rev. C5  
 (1972) 234

Tas 56 L.J. Tassie; Austral. J. Phys. 9 (1956) 407

Tas 73 L.J. Tassie; Austral. J. Phys. 26(1973) 433

Ter 73 T. Terasawa, M. Tanifugi and O. Mikoshiba;  
 Nucl. Phys. A203 (1973) 225

Weis 70 D.C. Weisser, J.S. Lilley, R.K. Hobbie and G.W. Greenlees  
 Phys. Rev. C2 (1970) 544

Ynt 67 J.L. Yntema and G.R. Satchler; Phys. Rev. 161 (1967) 1137

Appendix

Elimination of discrete ambiguities in the nuclear potential for elastic  $\alpha$ -particle scattering at higher energies

In the past few years the elastic  $\alpha$ -particle scattering has been measured at higher bombarding energies up to 166 MeV [Reed 68, Haus 69, Sin 69, Tat 70, Bach 72, Gol 73, Smi 73, Pu 74], and in some cases more extensive angular ranges. It has been argued that if the  $\alpha$ -particle penetrability increases faster with energy than the absorption the scattering probes the interior region of the potential and determines it more uniquely. For example, Hauser et al. [Haus 69], in a study of a dozen nuclei ranging from  ${}^6\text{Li}$  to  ${}^{209}\text{Bi}$  at  $E_\alpha = 104$  MeV, found for lighter nuclei a single discrete parameter set of the Saxon-Woods-potential characterized by a real depth of about 100 MeV. Furthermore these authors found some indications, in particular for  ${}^{12}\text{C}$ , that a wine-bottle potential represents the data better than the usual

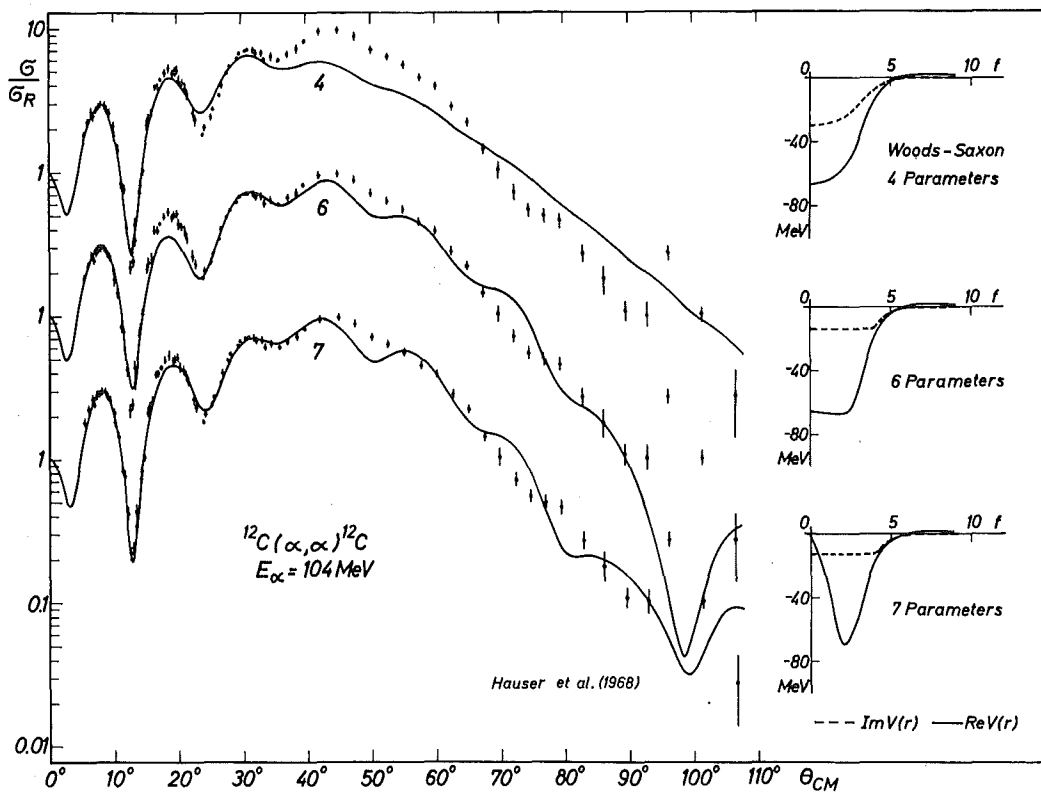


Fig. A1: Influence of the shape of the optical potential at small interaction distances on the elastic scattering of 104 MeV  $\alpha$ -particles from  ${}^{12}\text{C}$

Saxon-Woods-form (see fig. A1). For forward angles  $^{58}\text{Ni}$  data taken at  $E_\alpha = 64$  MeV Weisser et al. [Weis 70] found six equivalent potentials while 60-MeV measurements by Madland et al. [Madl 74] covering  $10^\circ$ -  $165^\circ$  resulted in only two equivalent potentials. Goldberg and Smith [Gol 72, Gol 73] obtained only a single "family" which adequately described their  $^{58}\text{Ni}$  data measured at 139 MeV within the forward hemisphere. Several authors [Gol 72, Sin 72] investigated the criteria for elimination of discrete ambiguities. These are

- a) that the energy is high enough for the cross section to exhibit an exponential decrease beyond a certain critical angle  $\theta_R$  and
- b) that the measurements must be continued beyond this angle.

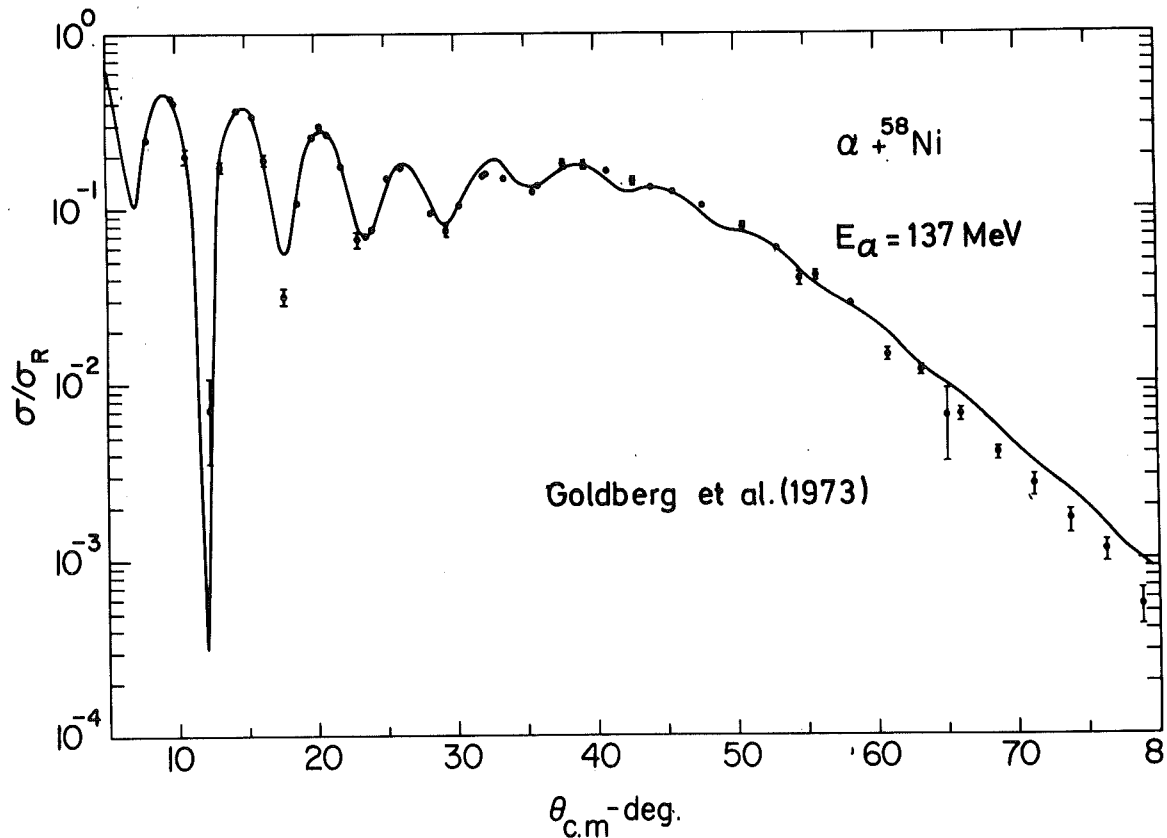


Fig. A2:  $^{58}\text{Ni}$  elastic scattering differential cross section as ratio to Rutherford scattering at  $E_\alpha = 139$  MeV [Gol 73]. The theoretical curve is an  $\alpha$  optical model fit.

Fig. A2 displays as example the differential cross section  $^{58}\text{Ni}(\alpha, \alpha)^{58}\text{Ni}$  at 139 MeV plotted as a ratio to the Rutherford cross section. The characteristic monotonic almost exponential fall-off pattern beyond a critical angle can be explained on the basis of a semiclassical description [Gol 72, Gol 73] revealing the origin of the disappearance of the discrete ambiguities.

In the classical limit the differential cross section is given by the familiar relation

$$\frac{d\sigma}{d\Omega}(\theta) = \frac{b}{\sin \theta} \frac{d\theta}{db}$$

where  $b$  is the impact parameter and  $\theta$  the deflection angle. The deflection angle is a function of the strength of the interaction, the projectile energy and the impact parameter. If the central depth of the interaction potential is large compared to incident energy, "spiral" scattering will occur, i.e. for some impact parameters, the deflection angle will exceed  $180^\circ$ . Provided that the interaction potential is approximately energy independent spiral scattering will cease to occur, if the energy is increased sufficiently. The scattering will then be characterized by a maximum deflection angle  $\theta_R$  (corresponding to the "rainbow" angle, of the Ford-Wheeler model [Eis 61, For 59]). It is intuitively clear, that a measurement of this angle can be used for a determination of the strength of the interaction. Classically no particles will be expected beyond this angle; the observed fall-off pattern is due to the wave properties of the scattering process.

The observed features of the elastic differential cross section have been called 'refractive behaviour' (in contrast to the diffraction like pattern at forward angles) and are discussed in an optical analogy in terms of a spatially varying complex refractive index [Gol 74]. The  $A$ - and energy dependence of the discrete ambiguities ("phase ambiguity") of the optical potential are explained by examination of the effective potentials  $V_{\text{eff}}(r, \ell) = U(r) + V_{\text{Coul}} + \frac{\hbar \ell(\ell+1)}{2mr^2}$  at the classical turning points for particles with angular momentum values  $\ell$ .

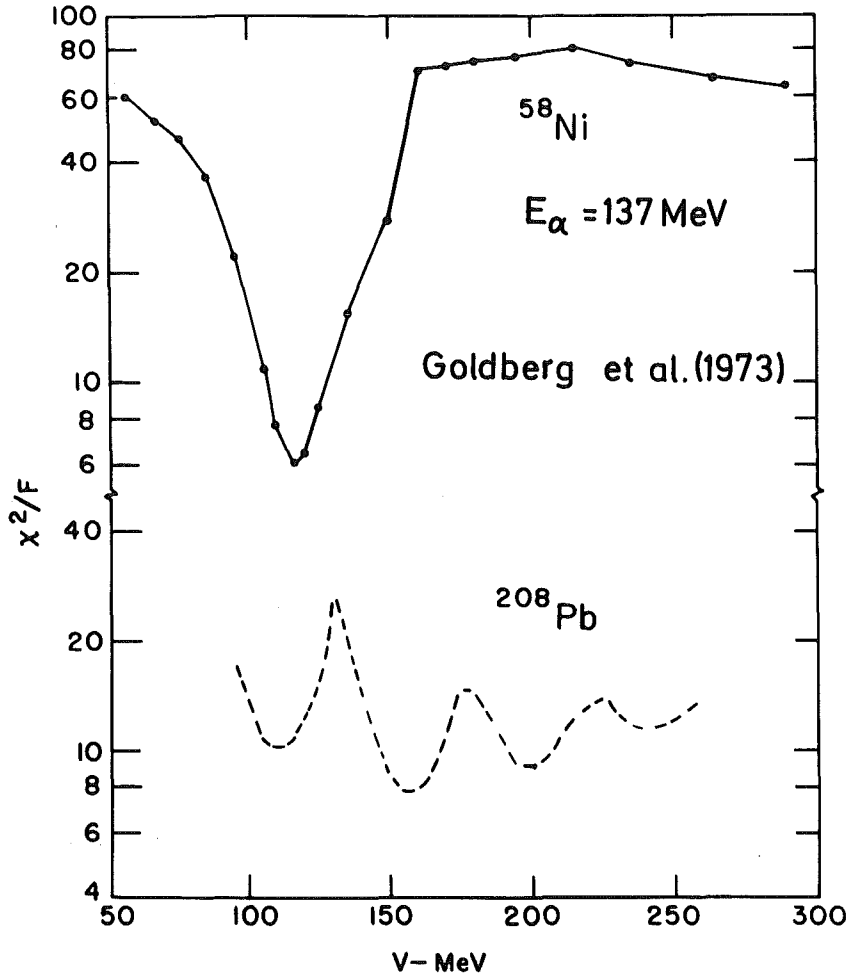


Fig. A3: Values of  $\chi^2/F$  for  $^{58}\text{Ni}(\alpha,\alpha)^{58}\text{Ni}$  and  $^{208}\text{Pb}(\alpha,\alpha)^{208}\text{Pb}$  at  $E_\alpha = 137$  MeV obtained from an optical model analysis [Gol 73]

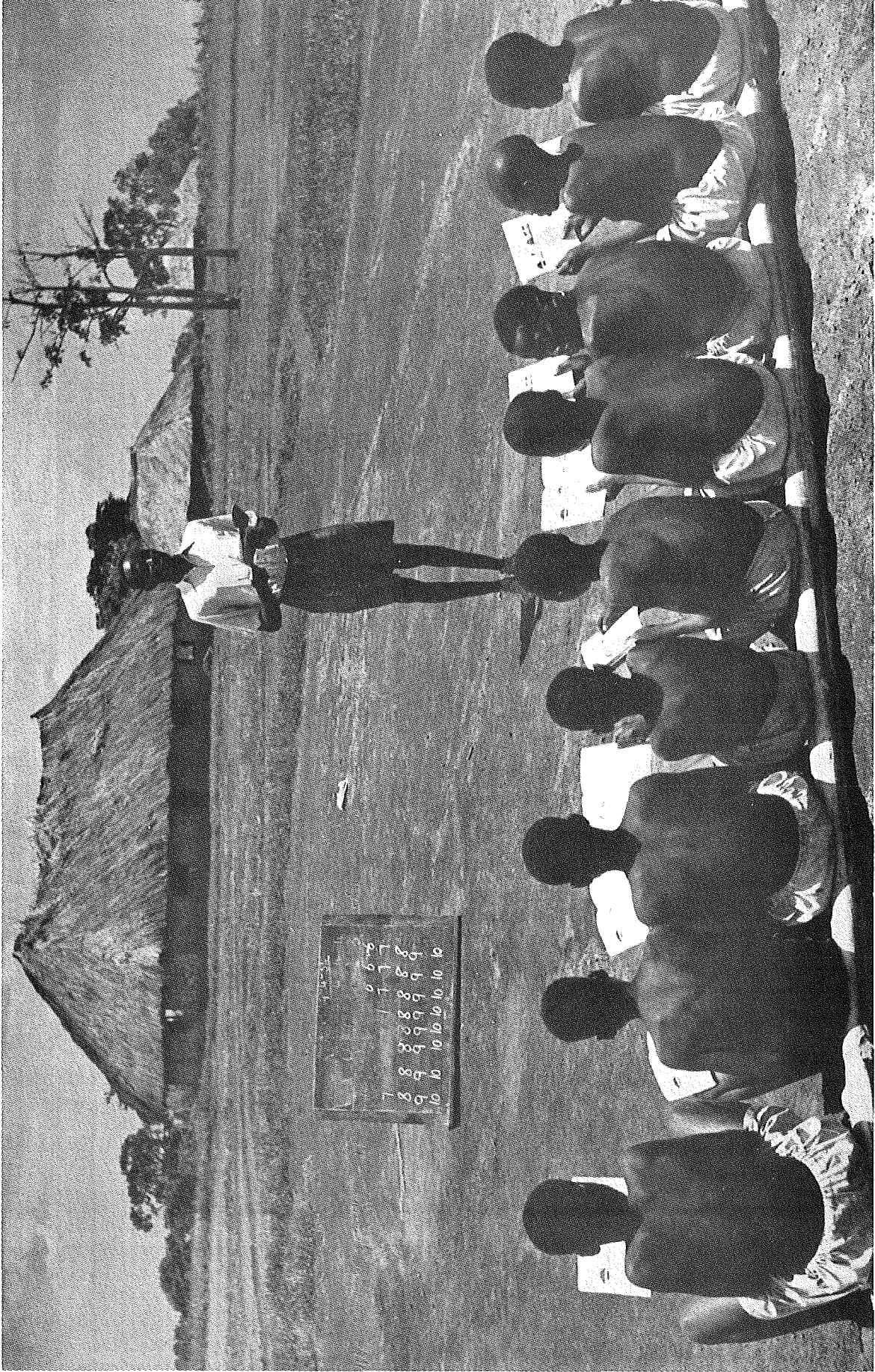
Fig. A3 shows for a optical model analysis of the elastic scattering of 137 MeV  $\alpha$ -particles on  $^{58}\text{Ni}$  and  $^{208}\text{Pb}$  the values of  $\chi^2/F$  obtained for different values of the real potential depth. For  $^{58}\text{Ni}$  the discrete ambiguity disappears while - in agreement with the more quantitative formulation of the criteria for elimination - a higher energy is required to remove ambiguities for the case of  $^{208}\text{Pb}$ . As in many other examples [Du 68, Haus 69, Tat 70, Re 72b, Re 72c, Pu 74] the best fit value of the real potential depth is in the vicinity of  $V_0 = 100-130$  MeV. There seems to be a tendency of increasing the strength  $V_0$  with the atomic number  $A$ . This may be also indicated by the  $^{208}\text{Pb}$  example of fig. A3 even if it cannot be decided unambiguously which

$\chi^2$ -minimum represents the "true" potential. \*)

Recently Put and Paans [Pu 74] performed detailed investigations for elastic  $\alpha$ -particle scattering from  $^{90}\text{Zr}$  at several energies  $E_\alpha = 40$ -118 MeV and over a wide angular range. The optical model analysis for the 118 MeV data result in a parameter set with  $V_o = 130$  confirming the prediction on the basis of the arguments of Goldberg and Smith. With only slightly different values of real and imaginary depths the found parameter set gives the best fit to the data also at lower energies  $E_\alpha > 79.5$  MeV. For  $E_\alpha < 79.5$  MeV a distinct "break" in the energy dependence of the shape parameters of the potential is observed. The "true" potential seems to be distorted by exchange effects or by terms representing virtual excitation in the generalized optical potential [Fes 58]. This would imply that perhaps the folding approach works well at higher energies, but is rather poor at lower energies.

---

\*) The result [Ta 70] quoting  $V_o = 118$  MeV at  $E_\alpha = 166$  MeV seems not to be conclusive because of the restricted angular range and reduced angular accuracy of the measurements.



SUMMERSCHOOL